Journal of Translational Medicine

RESEARCH

Open Access

ML335 inhibits TWIK2 channel-mediated potassium efflux and attenuates mitochondrial damage in MSU crystal-induced inflammation

Dianze Song[1], Xiaoqin Zhou[1], Qingqing Yu[1], Renjie Li[1], Qian Dai[1,2*†] and Mei Zeng[1,2,3*†]

Abstract

Background Activation of the NLRP3 inflammasome is critical in the inflammatory response to gout. Potassium ion (K^+) efflux mediated by the TWIK2 channel is an important upstream mechanism for NLRP3 inflammasome activation. Therefore, the TWIK2 channel may be a promising therapeutic target for MSU crystal-induced inflammation. In the present study, we investigated the effect of ML335, a known K2P channel modulator, on MSU crystal-induced inflammatory responses and its underlying molecular mechanisms.

Methods By molecular docking, we calculated the binding energies and inhibition constants of five K2P channel modulators (Hydroxychloroquine, Fluoxetine, DCPIB, ML365 and ML335) with TWIK2. Intracellular potassium ion concentration and mitochondrial function were assessed by flow cytometry. The interaction between MARCH5 and SIRT3 was demonstrated by immunoprecipitation and Western blotting assay. MSU suspensions were injected into mouse paw and peritoneal cavity to induce acute gout model.

Results ML335 has the highest binding energy and the lowest inhibition constant with TWIK2 in the five calculated K2P channel modulators. In comparison, among these five compounds, ML335 efficiently inhibited the release of IL-1β from MSU crystal-treated BMDMs. ML335 decreased MSU crystal-induced K^+ efflux mainly dependent on TWIK2 channel. More importantly, ML335 can effectively inhibit the expression of the mitochondrial E3 ubiquitin ligase MARCH5 induced by MSU crystals, and MARCH5 can interact with the SIRT3 protein. ML335 blocked MSU crystal-induced ubiquitination of SIRT3 protein by MARCH5. In addition, ML335 improved mitochondrial dynamics homeostasis and mitochondrial function by inhibiting MARCH5 protein expression. ML335 attenuated the inflammatory response induced by MSU crystals in vivo and in vitro.

†Qian Dai and Mei Zeng have contributed equally to this work and share corresponding authorship.

*Correspondence:
Qian Dai
daiqian@nsmc.edu.cn
Mei Zeng
zengmei123@gmail.com

Full list of author information is available at the end of the article

Conclusion Inhibition of TWIK2-mediated K^+ efflux by ML335 alleviated mitochondrial injury via suppressing March5 expression, suggesting that ML335 may be an effective candidate for the future treatment of gout.

Keywords ML335, MSU crystal, TWIK2, MARCH5, SIRT3, Mitochondrial function

Introduction

Gout is a highly prevalent disease [1, 2] and is induced by the crystalline deposition of monosodium urate (MSU) in the joints and/or surrounding tissues [3]. There is a lack of specialized curative treatment for gouty arthritis (GA), and current treatment options focus on the treatment of acute exacerbations and the provision of effective long-term maintenance treatment [4]. Urate-lowering drugs and anti-inflammatory drugs are commonly used in GA clinical treatment [5]. These existing therapeutic drugs only alleviate symptoms or delay the occurrence of GA and even have a large number of adverse effects, which may be the cause of GA recurrence [6]. The lack of reliable therapeutic targets has challenged and delayed the development of targeted drugs for the treatment of GA [7].

NLRP3 inflammasome assembly facilitates IL-1β/IL-18 secretion and triggers pyroptosis; consequently, activation of the NLRP3 inflammasome has been related to a variety of human diseases, including gout, Alzheimer's disease and diabetes [8]. Dysregulated expression of NLRP3 inflammasome members and aberrant activation of the NLRP3 inflammasome are frequently found in gouty animal models and GA patients [9, 10]. Activation of the NLRP3 inflammasome requires two signals: priming signal and activation signal. Saturated long-chain fatty acids (LCFAs), for instance, stearic acid (C18:0) and palmitic acid (C16:0), deliver priming signals and synergize with MSU crystals to facilitate the activation of the NLRP3 inflammasome [11]. It is essential to block the sustained activation of the NLRP3 inflammasome with multiple therapeutic agents, which could be developed as an effective way to treat or prevent GA [12].

Potassium (K^+) efflux is a significant upstream mechanism for the stimulation of the NLRP3 inflammasome by most NLRP3 agonists [13–15]. A variety of NLRP3 agonists trigger potassium efflux mechanistically via distinct pathways [15]. A massive increase in extracellular ATP to tens or hundreds of micromoles/liter in dying or stressed cells activates the NLRP3 inflammasome through linkage to purinergic P2×7 receptors [16, 17]. TWIK2 (KCNK6) channels are in the TWIK subfamily of two-pore structural domain potassium channels that mediate potassium efflux in cooperation with P2×7 receptors and underlie the NLRP3 inflammasome induced by ATP. Lack of TWIK2 prevented lung inflammation induced by sepsis in vivo and NLRP3 activation induced by ATP in vitro [18, 19]. Endosomal trafficking of TWIK2 to the plasma induces NLRP3 inflammasome activation and inflammatory injury [20]. Suppression of S1PR3 inhibits ATP-induced NLRP3 inflammasome activation in macrophages via potassium efflux mediated by TWIK2 [21]. ML365 inhibition of TWIK2 channels blocks the ATP-induced NLRP3 inflammasome [22]. However, either the effects of K2P channel modulators or TWIK2 on MSU crystal-induced inflammation are poorly studied. In the present study, we focused on the effects of K2P channel modulators (ML335) on MSU crystal-induced NLRP3 inflammasome activation and the underlying molecular mechanisms.

Materials and methods

Molecular modeling study of TWIK2 with the K2P regulator

We used the open-source molecular docking software Autodock4.2 to perform molecular docking studies on the five K2P regulators. First, homology modeling was conducted with the Swiss-model (https://swissmodel.expasy.org/interactive) to obtain the protein structure of the macromolecular receptor, and then polar hydrogen was added to the crystals of the receptor protein by Autodock4.2. After obtaining the macromolecular receptor, the chemical structure formula of the small molecule ligand needs to be drawn in Chemdraw, and later, the minimum energy conformation of small molecules must be calculated in Chem3D for molecular docking. After the small molecule ligand and macromolecular receptor files are prepared, the rotatable atoms need to be defined in Autodock 4.2 software, and later, the small molecule ligand is embedded in the macromolecular receptor with the Autogrid, where the coordinates of the embedding site are typically those of the original similar small molecule ligand. After embedding, the small molecule ligand is docked to the large molecule receptor using the Autodock program, which is typically run 100 times. When the results are analyzed, the conformation with the lowest energy and the largest number of clusters is generally chosen as the dominant conformation for the discussion of the results.

Reagents

Hydroxychloroquine(HCQ), Fluoxetine, DCPIB, ML365, ML335 and MG132 were purchased from MedChemExpress (China).

Preparation of fatty acids (FAs, palmitic acid and stearic acid)

Palmitic and stearic acids were prepared as described previously [11]. The detailed procedure was supplied in the supplementary information.

Cell culture, MSU crystals preparation and cell treatment

Primary mouse BMDMs were taken from the bone marrow of C57BL/6 mice at 6–8 weeks of age, differentiated in DMEM (PM150210, Procell Life Science & Technology Co.,Ltd, China) with 10% FBS (164210-50, Procell Life Science & Technology Co., Ltd, China) and 20 ng/mL M-CSF(315-02, PeproTech Technology Co., Ltd, China), and treated 7–10 days after separation. The preparation of MSU crystal (MSUc) was performed as described previously [23]. The detailed procedure for the preparation of MSU crystals were supplied in the supplementary information. To explore the appropriate concentration of five K2P channel modulators to inhibit IL-1β secretion, BMDMs were pretreated with different concentration (1, 5, 10μM) of DCPIB, Fluoxetine, ML335, ML365 and HCQ for 1 h, then stimulated with FAs (5 μM)+MSUc (50 μg/ml) for 12 h. In subsequent experiments, BMDMs were pretreated with 5 μM ML335 for 1 h, and then stimulated with FAs (5 μM)+MSUc (50 μg/ml) for 12 h.

ELISA

IL-1β, TNFα, IL-6 and CCL2 were measured in culture supernatants or peritoneal lavage fluid using ELISA kits (IL-1β, EMC001b), (TNFα, EMC102a), (IL-6, EMC004), (CCL2, EMC113), (NeoBioscience Technology Co., Ltd, China).

Table 1 The sequences of primer for PCR amplification

Gene	Forward primer (5′-3′)	Reverse primer (5′-3′)
Mice D-loop	AATCTACCATCCTCCGTGAA ACC	TCAGTTTAGCTACCCC CAAGTTTAA
Mice 18 S	TAGAGGGACAAGTGGCGTTC	CGCTGAGCCAGTCA GTGT
Mice Tert	CTAGCTCATGTGTCAAGACC CTCTT	GCCAGCACGTTTCTC TCGTT
Mice Cox	GCCCCAGATATAGCATTCCC	GTTCATCCTGTTCCT GCTCC
Mice Non-Numt	CTAGAAACCCCGAAACCAAA	CCAGCTATCACCAAG CTCGT
Mice B2m	ATGGGAAGCCGAACATACTG	CAGTCTCAGTGGGGG TGAAT
Mice March5	GACTGATCTCAAAAGCTTGCC	CTCCATAACATCCAGC CCTTC
Mice KCNK6	TTCATCTCTCAGTCCACCATTG	CGGAAAGTCTGCAAC ACGAG
Mice LKB1	CGAGGGATGTTGGAGTATGAG	CTTAGTGTCTGGGCT TGGTG
Mice GAPDH	CTTTGTCAAGCTCATTTCCTGG	TCTTGCTCAGTGTCC TTGC

Isolation of mitochondrial proteins and determination of mitochondrial SOD activity

Mitochondria were isolated from BMDMs using the Cell Mitochondria Isolation Kit (C3601, Beyotime Biotechnology, China) and then RIPA was added to obtain mitochondrial proteins. The Cu/ZnSOD and Mn-SOD Assay Kit of WST-8 (S0103, Beyotime Biotechnology, China) was employed for the determination of mitochondrial SOD activity in mitochondrial proteins. The mitochondrial proteins concentration was assayed utilizing the BCA Protein Assay Kit (P0009, Beyotime Biotechnology, China). The SOD activity of the sample was expressed as the ratio of the detected SOD activity to the protein concentration.

Transfection experiments

The plasmids of pcDNA3.1(+)-mSirt3-Myc, pcDNA3.1(+)-mMarch5-HA, pcDNA3.1(+)-mKcnk6, pcDNA3.1(+)-Ub-HA, CRISPR v2-mMarch5, CRISPR v2-mLKB1 were obtained from the Public Protein/Plasmid Library (China). Plasmid transfection was implemented with Lipo8000 kits (C0533, Beyotime Biotechnology, China), respectively, following the manufacturer's instructions. The expression levels of related gene were verified by RT-qPCR after plasmid transfection of BMDMs for 36 h. The detailed procedure of RT-qPCR assay is supplied in the supplementary information. The primer sequences for the corresponding genes are shown in the Table 1. BMDMs were transfected with the corresponding plasmids for 36 h, followed by pretreatment with ML335 for 1 h and then stimulation with MSU for 12 h before performing the relevant experiments.

Western blot analysis

Pro-IL-1β and pro-caspase-1 processing was detected by Western blotting. Cell culture supernatants were collected and precipitated in deoxycholate containing 20% trichloroacetic acid (TCA) and washed three times with 100% acetone, before concentration in 1× Laemmli buffer. Mice paw tissues and BMDMs were lysed with RIPA buffer. Later, the concentration of protein was measured via the BCA Protein Assay Kit (P0009, Beyotime Biotechnology, China). The Western blot assay procedure is described in the supplementary information and the information of antibodies is described in the Table 2. The Western blotting assay was repeated three times to analyze with densitometry using Image J software and show representative bands.

Ultrastructural observation

After various interventions, BMDMs were rinsed three times using 1×PBS and fixed in 2.5% glutaraldehyde overnight. Mitochondrial morphology was analyzed using TEM, and mitochondrial crista density was calculated

Table 2 The antibodies were used in Western blotting or immunofluorescence assays

Antibodies	Source	Identifier
Recombinant Rabbit Anti-beta TUBULIN	HUABIO	Cat#ET1602-4
Rabbit monoclonal CMPK2	ImmunoWay	Cat#YT6811
Recombinant Rabbit Anti-VINCULIN	HUABIO	Cat#ET1705-94
Rabbit monoclonal AMPKα	HUABIO	Cat#ET1608-40
Rabbit monoclonal P-DRP1	CST	Cat#S616
Rabbit monoclonal Anti-DRP1	HUABIO	Cat#HA500487
Rabbit monoclonal COX2	HUABIO	Cat#ET1610-23
Recombinant Rabbit Anti-GAPDH	HUABIO	Cat#ET1601-4
Rabbit monoclonal Anti-MFF	HUABIO	Cat#ER1902-93
Rabbit monoclonal P-LKB1	CST	Cat#S428
Rabbit Polyclonal LKB1	HUABIO	Cat#HA500143
Rabbit monoclonal KCNK6	HUABIO	Cat#HA500213
Rabbit monoclonal Ubiquitin Rabbit	PTMab	Cat#ptm-1106RM
Rabbit monoclonal Acetylly-sine Rabbit	PTMab	Cat#PTM-105RM
Rabbit monoclonal ARG1	HUABIO	Cat#ET1605-8
Rabbit monoclonal INOS	Abcam	Cat#ab178945
Rabbit monoclonal ARG2	HUABIO	Cat#ET7110-91
Rabbit monoclonal FIS1	proteintech	Cat#10956-1-AP
Rabbit monoclonal MFN1	HUABIO	Cat#ET1702-01
Rabbit monoclonal MFN2	HUABIO	Cat#ER1802-23
Rabbit monoclonal OPA1	HUABIO	Cat#ET1705-9
Rabbit monoclonal March5	ImmunoWay	Cat#YT2646
Rabbit monoclonal SOD2/MnSOD	Abcam	Cat#AB137037
Rabbit monoclonal HADH	HUABIO	Cat#R1411-4
Rabbit monoclonal ACADL	proteintech	Cat#17526-1-AP
Rabbit monoclonal HA	AlpaVHHs	Cat#003-201-001
Rabbit monoclonal MYC	AlpaVHHs	Cat#002-203-001
Rabbit monoclonal CD36	HUABIO	Cat#ET1701-24
Rabbit monoclonal FAS	HUABIO	Cat#ET1701-91
Rabbit monoclonal P-ACC1	CST	Cat#SER79
Rabbit monoclonal ACC1	HUABIO	Cat#ET1609-77
Rabbit monoclonal SIRT3	Bioworld	Cat#BS7772
Rabbit monoclonal CPT2	HUABIO	Cat#ET1611-64
Rabbit monoclonal MPO	Abcam	Cat#ab208670
Rabbit monoclonal P-AMPK	CST	Cat#T172(40H9)
Rabbit polyclonal NLRP3	HUABIO	Cat#ER1706-72
Rabbit monoclonal CPTIA	Abcam	Cat#ab234123
Mouse monoclonal IL-Iβ	CST	Cat#3A6
Mouse monoclonal Caspase-1	AdipoGen	Cat#AG-20B-0042
Rabbit monoclonal CD11b	BOSTER	Cat#BEM3925

using the following formula: the sum of the total crista volume divided by the sum of the mitochondrial areas as described previously [24].

Immunoprecipitation

The detailed experimental procedure of immunoprecipitation is described in the supplementary information.

Analyses of mitochondrial morphology

The Mito-Tracker Green probe (C1048, Beyotime Biotechnology, China) staining was used to observe the mitochondrial morphology of BMDMs. After various interventions, BMDMs were rinsed twice using 1×PBS and subsequently incubated utilizing Mito-Tracker Green for 30 min in 37℃. After rinsing twice with 1×PBS, the cells were stained with Hoechst33342 (40731ES, YEASEN, China) for 10 min, and then the mitochondrial morphology was observed by applying a laser confocal microscope (Olympus, FV3000, Japan). The aspect ratio (AR) is the ratio between the minor and major axes corresponding to the elliptical shape of the mitochondria.

Measurements of intracellular total reactive oxygen species (ROS) and mitochondrial ROS

The intracellular total ROS and mitochondrial ROS were respectively performed following the manufacturer's instructions. The detailed procedure was described in the supplementary information.

Detection of mitochondrial membrane potential (ΔΨm)

ΔΨm was examined by a JC-1 fluorescent probe (C2003S, Beyotime, China). BMDMs were washed twice in 1×PBS and stained with 1:200 JC-1 working buffer for 30 min at 37 °C. Then, the cells were washed with 1×PBS again, and analyzed by flow cytometry (SA3800, Sony, Japan). As for laser confocal microscopy analysis, nuclei were stained with Hoechst33342.

Detection of intracellular potassium ion concentration

Intracellular potassium ion concentrations were examined by Enhanced Potassium Green-2 AM (EPG-2 AM, MX4513, Maokang Biotechnology, Shanghai, China), a fluorescence probe for intracellular potassium ions. The optimal excitation wavelength for EPG-2 AM is 517 nm. BMDMs were washed twice with 1×PBS and loaded with 5 μM EPG-2 AM for 30 min, after which the cells were washed twice with 1×PBS and analyzed with flow cytometry.

Quantitative analysis of mitochondrial respiration

A Seahorse XF24 extracellular flux analyzer (Agilent Seahorse Biosciences) was applied to detect cellular respiration. Each well was inoculated with 20,000 cells. Cells were incubated in DMEM for an hour and then replaced

with prewarmed XF assay medium, and the oxygen consumption rate (OCR) was assayed with a Seahorse XF kit (103015-100, Agilent Seahorse, China). The first block tested was the basal respiration rate. The analysis of respiration rate was performed by stepwise injections of mitochondrial complex inhibitors such as 0.5 μM rotenone-antimycin A, 2 μM FCCP, and 1.5 μM oligomycin A as per the manufacturer's protocol.

Measurement of mitochondrial DNA (mtDNA) content and oxidized mtDNA

The TIANamp Genomic DNA kit (DP304-02, TIANGEN, China) was used for the isolation of total DNA according to the manufacturer's instructions. Quantification of mtDNA via qPCR with primers specific to the mitochondrial D-loop region, cytochrome c oxidase (Cox1), or specific mtDNA regions not inserted into the nuclear DNA (non-NUMT). B2m, 18 S ribosomal RNA and nuclear DNA encoding Tert were employed for normalization. The sequences of all primers are shown in the Table 1.

For the measurement of oxidized mitochondrial DNA (Ox-mtDNA), purified mtDNA was extracted from mitochondrial fractions as indicated. The 8-OHdG content was then quantified using 8-hydroxydeoxyguanosine ELISA Kit (Elabscience Biotechnology Co., Ltd, China) according to manufacturer's instructions.

Flow cytometry for macrophage subset analysis

To explore the effects of ML335 treatment on macrophage M1 and M2 polarization, CD86 was chosen to mark the M1 phenotype and CD206 for the M2 phenotype. Alexa APC-conjugated anti-CD86 (E-AB-F0994E, Elabscience, China) and FITC conjugated anti-206 (E-AB-F1135C, Elabscience, China) were used to evaluate macrophage subsets. BMDMs were stimulated with lipopolysaccharide (20 ng/mL) plus IFN-g (50 ng/mL) for 6 h for M1 polarization, or with IL-4 (20 ng/mL; PeproTech) for 12 h for M2 polarization. BMDMs were pretreated with ML335 for 1 h, and then stimulated with FAs + MSUc for 12 h for M1 polarization.

Metabolite profiling analysis

BMDMs were intervened, and then, metabolomic assay and analyses were performed at Wuhan MetWareBiotech Co. Ltd. (China), and the detailed procedure of metabolomic assay is supplied in the supplementary information.

Mice model

C57BL/6J mice (8–10 weeks, 20–25 g) were purchased from GemPharmatech (Chengdu, China). Sterile PBS (40 μL) was injected into the right paw as a control, and MSU suspension (40 μL, 1 mg of MSU crystals in 40 μL of physiological saline) were injected into the left paw as the experimental group. A Vernier caliper was utilized to examine the degree of swelling of the paw. The index of paw swelling was expressed as the ratio of the thickness of the paw injected with MSU suspension to that injected with PBS. To establish a mouse model of peritonitis induced by MSU crystals, mice were injected intraperitoneally with MSU suspension (3 mg of MSU crystals in 0.5 ml of PBS), and six hours later, the mice were executed under carbon dioxide anesthesia, and the peritoneal lavage fluid was extracted. After the peritoneal lavage fluid was centrifuged, the supernatants were utilized for ELISA, and the precipitates were stained with proper antibodies (CD45, BD Bioscience, 553,080; F4/80, BD Bioscience, 565,410; CD11b, Biolegend, 101,263; Ly6G, Biolegend, 127,613) for flow cytometry detection.

Histological studies and immunofluorescence

Mouse paw tissues were paraffin-embedded and sliced into 5-μm-thick sections for immunofluorescence and hematoxylin-eosin (HE) staining. The detailed procedures for paraffin tissue sections and cell immunofluorescence were supplied in the supplementary information. The information about the antibodies used in the immunofluorescence assay was supplied in the Table 2.

Statistical analysis

Values are presented as the mean ± standard deviation (SD). One-way ANOVA was applied for statistical analysis. All of the statistical analyses were calculated by utilizing GraphPad Prism software (Version 6.0). Analyses between two groups were performed using the Student's t-test. For comparisons among more than two groups, one-way ANOVA followed by Tukey's post hoc test was used. The symbols in the graphs denote significantly different groups as follows: $^{*}P<0.05$; $^{**}P<0.01$.

Results

ML335 suppressed FAs + MSUc-induced NLRP3 inflammasome activation

To identify the interacting mode of KCNK6 with five known K2P channel modulators (DCPIB, Fluoxetine, HCQ, ML335 and ML365), molecular docking study was performed. The data were shown in Fig. S1. We also calculated the binding energies and Ki values of the five compunds to KCNK6 by molecular docking. The data indicated that ML335 has the highest calculated binding energy to TWIK2 and the lowest Ki values among the five compounds (Table 3). Previous studies have suggested that TWIK2 channels are promising drug targets for NLRP3-associated inflammation. This prompted us to explore the effects of five known K2P modulators on IL-1β secretion in BMDMs treated with FAs + MSU crystal. The IL-1β level was measured in BMDMs exposed to different doses of five K2P modulators (1, 5 and 10 μM)

Table 3 The calculated binding energies and Ki values of compounds with KCNK6

Compound	Calculated binding energies (kcal/mol)	Calculated Ki(μM)
hydroxychloroquine	-9.15	0.197
DCPIB	-9.52	0.105
fluoxetine	-8.86	0.317
ML335	-10.72	0.013
ML365	-9.02	0.243

followed by treatment with FAs+MSUc crystals. As shown in Fig. S2A, among the five compounds tested, HCQ showed the best inhibition of IL-1β secretion at 1 μM, and the remaining four compounds were 5μM. We further compared the effects of five compounds on IL-1β secretion. ML335 inhibited IL-1β secretion more effectively than Fluoxetine. Compared to the other three compounds, the mean value of IL-1β levels was the lowest after ML335 treatment, but there was no statistical difference among them (Fig. 1A). Based on these data, we focused on the role of ML335 and its potential anti-inflammatory molecular mechanisms in this study. KCNK6 overexpression impeded the effect of ML335 on FAs+MSUc-induced IL-1β secretion (Fig. 1B). Since IL-1β secretion is mainly influenced by post-translation, we further investigated the effects of ML335 on NLRP3 protein levels and NLRP3 inflammasome activation. ML335 decreased NLRP3 protein levels induced by

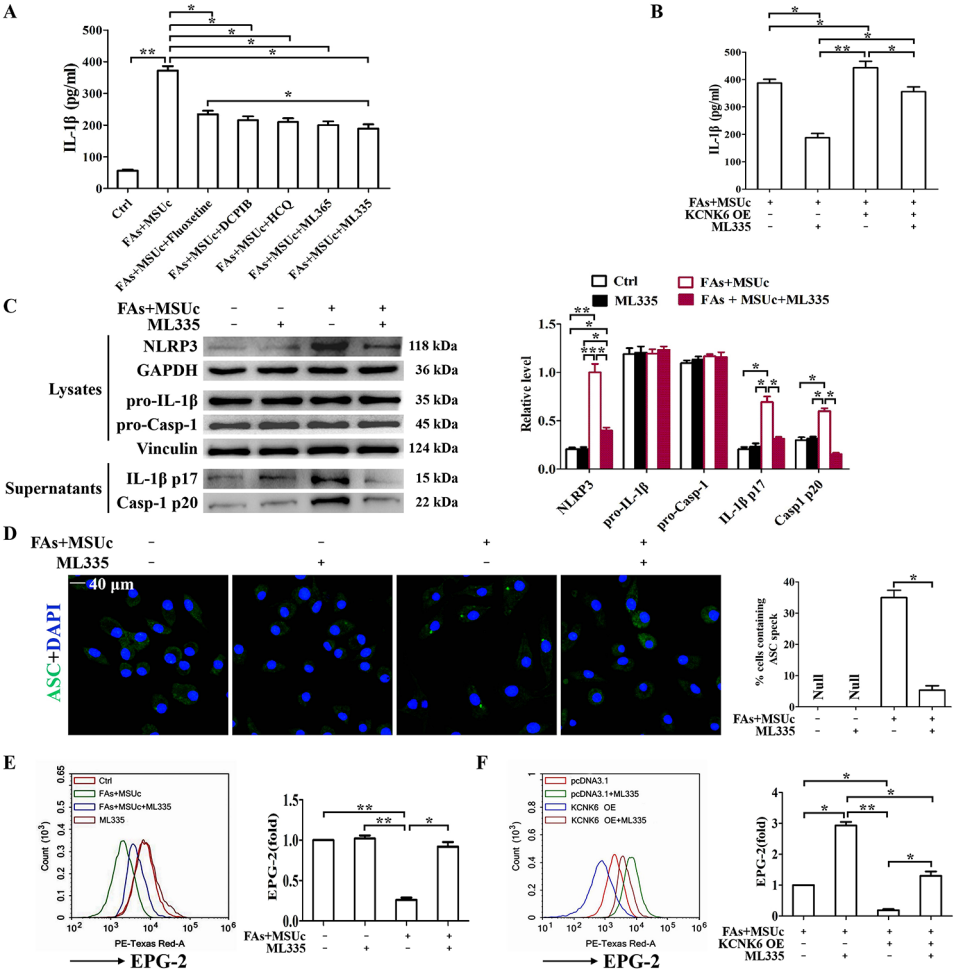

Fig. 1 ML335 inhibited NLRP3 inflammasome activation and increased intracellular potassium concentration in BMDMs treated with FAs+MSUc. (**A**) ELISA assay to detect the effect of Fluoxetine, DCPIB, HCQ, ML365 and ML335 treatments on IL-1β levels in culture supernatants. (**B**) The inhibitory effect of ML335 on IL-1β secretion was blocked by KCNK6 overexpression as detected by ELISA. (**C**) Western blotting was used to detect NLRP3, pro-IL-1β, pro-Casp-1, protein levels in the lysates of BMDMs and IL-1β p17, Casp-1p20 protein levels in culture supernatants. The relative levels of NLRP3/GAPDH, pro-IL-1β/Vinculin, pro-Casp-1/Vinculin, IL-1β p17/ Vinculin, Casp-1p20/ Vinculin were depicted on the right. (**D**) Immunofluorescence detection was used to examination ASC speck formation. Hoechst33342 stains nucleus. Scale bar: 40 μm. Null means no fluorescence signal. (**E**) Enhanced Potassium Green-2 (EPG-2) staining and flow cytometry analysis of the effect of ML335 on intracellular potassium ion concentration. The relative fluorescence intensity of EPG-2 was displayed on the right. (**F**) EPG-2 staining and flow cytometry analysis of KCNK6 overexpression reversed ML335 inhibition of intracellular potassium efflux. The relative fluorescence intensity of EPG-2 was displayed on the right

FAs+MSUc, but had no effect on pro-IL-1β and pro-Casp-1 expression (Fig. 1C). Importantly, ML335 suppressed the activation of the NLRP3 inflammasome induced by FAs+MSU crystals in BMDMs, as proven by decreased levels of active Caspase-1 (Casp-1 p20) and mature IL-1β (IL-1β p17) in cell supernatants (Fig. 1C). In the same supernatants, ML335 attenuated the TNF-α and IL-6 levels, which are closely associated with inflammation induced by MSU crystals (Fig. S2B). Immunofluorescence staining data showed that ML335 significantly decreased the number of FAs+MSUc-induced ASC specks, further reflecting that ML335 inhibited NLRP3 inflammasome activation (Fig. 1D). We further examined the effect of ML335 on the intracellular K^+ concentration. FAs+MSUc stimulation caused a decrease in K^+ concentration, which was reversed by ML335 (Fig. 1E). KCNK6 overexpression blocked the effect of ML335 on intracellular K^+ concentration (Fig. 1F). These data suggest that ML335 may up-regulate intracellular K+ concentration by inhibiting KCNK6 activity, which in turn inhibits NLRP3 inflammasome activation in FAs+MSUc induced inflammation.

ML335 mitigates oxidative stress and mitochondrial injury induced by FAs+MSUc

Mitochondrial dysfunction is central to the activation of the NLRP3 inflammasome. To examine whether the suppression of NLRP3 inflammasome activation by ML335 was attributable to rescue of mitochondrial damage induced by FAs+MSU crystal, we investigated the impact of ML335 on mitochondrial status. In contrast to the control group, FAs+MSUc boosted the production of intracellular total ROS (Fig. 2A) and mitochondrial ROS (Fig. 2B). ML335 pretreatment significantly reduced the FAs+MSUc-induced increase in intracellular total ROS (Fig. 2A) and mitochondrial ROS levels (Fig. 2B). It is well known that the loss of Δψm is related to mitochondrial ROS accumulation. Laser confocal microscope imaging and flow cytometry analysis of Δψm data showed that ML335 pretreatment promoted the ratio of red/green fluorescence, indicating an improved depolarization state of mitochondria (Fig. 2C and D). The exposure of newly synthesized mtDNA to ROS leads to oxidized mtDNA (ox-mtDNA) production, which is released into the cytoplasm, where it combines with NLRP3 and triggers NLRP3 inflammasome assembly. CMPK2 is a mitochondrial nucleotide kinase, the rate-limiting enzyme required to initiate mtDNA synthesis. We wonder whether ML335 affects CMPK2 protein levels, total mtDNA and ox-mtDNA levels. ML335 treatment inhibited CMPK2 protein expression (Fig. 2E), total mtDNA (Fig. S3A-S3B) and oxidized mtDNA levels (Fig. 2F) in response to FAs+MSUc, suggesting that ML335 treatment interfered with not only the synthesis of mtDNA but also mtDNA oxidation. Subsequently, the mitochondrial respiratory activity was identified by assaying the OCR of the BMDMs with a Seahorse XF24 Extracellular Flux Analyzer. Respiratory parameter determinations indicated that basal respiration, ATP production rate, maximum respiration rate, spare capacity and proton leak were higher in the FAs+MSUc+ML335 group than in the FAs+MSUc group (Fig. 2G). ML335 had no significant effect on non-mitochondrial respiration in BMDMs treated with FAs+MSUc. These data implied that ML335 ameliorated mitochondrial dysfunction induced by FAs+MSUc.

ML335 improves mitochondrial dynamics homeostasis and mitochondrial ultrastructure

Sirt3 is engaged in the modulation of mitochondrial kinetic remodeling. The dynamic balance between mitochondrial fission and fusion dictates mitochondrial morphology. We surveyed the effect of ML335 on mitochondrial morphology by live-cell imaging with MitoTracker dye. In the untreated cells, a number of mitochondria were filamentous and developed a network of interconnected tubes (Fig. 3A). During the treatment of FAs+MSUc, mitochondria was fragmented into short rods or spheres, and the mitochondrial network was also ruptured (Fig. 3A). ML335 treatment improves the structural integrity of mitochondria (Fig. 3A). For quantification, we established the aspect ratio (AR, the ratio of the major axis to the minor axis) of mitochondria in each group. We observed that FAs+MSUc stimulation induced a significant decrease in the mitochondrial AR value, which was significantly prevented by treatment with ML335, suggesting that mitochondrial fragmentation was decreased (Fig. 3A). Western blotting was performed to confirm the improved mitochondrial fission/fusion balance, which revealed that ML335 facilitated mitochondrial fusion (low levels of the fission proteins phosphorylated Drp1 (p-Drp1ser616), MFF, and Fis1 but high levels of the fusion proteins MFN1/2) (Fig. 3B). However, ML335 did not significantly ameliorate the FAs+MSUc-induced reduction of the mitochondrial fusion protein OPA1 (Fig. 3B). Specifically, immunofluorescence assay data indicated that FAs+MSUc exposure accelerated Drp1 translocation to mitochondria, and ML335 decreased the impact of FAs+MSUc on Drp1 mitochondrial translocation (Fig. 3C). In addition, the impacts of ML335 on the mitochondrial morphology of BMDMs treated with FAs+ML335 were further investigated by transmission electron microscopy (TEM). TEM images indicated that mitochondrial cristae were broken and mitochondrial cristae volume density was decreased in BMDMs stimulated by FAs+MSUc (Fig. 3D). Interestingly, ML335 protected against mitochondrial crista integrity damage by FAs+MSUc (Fig. 3D), the folds in

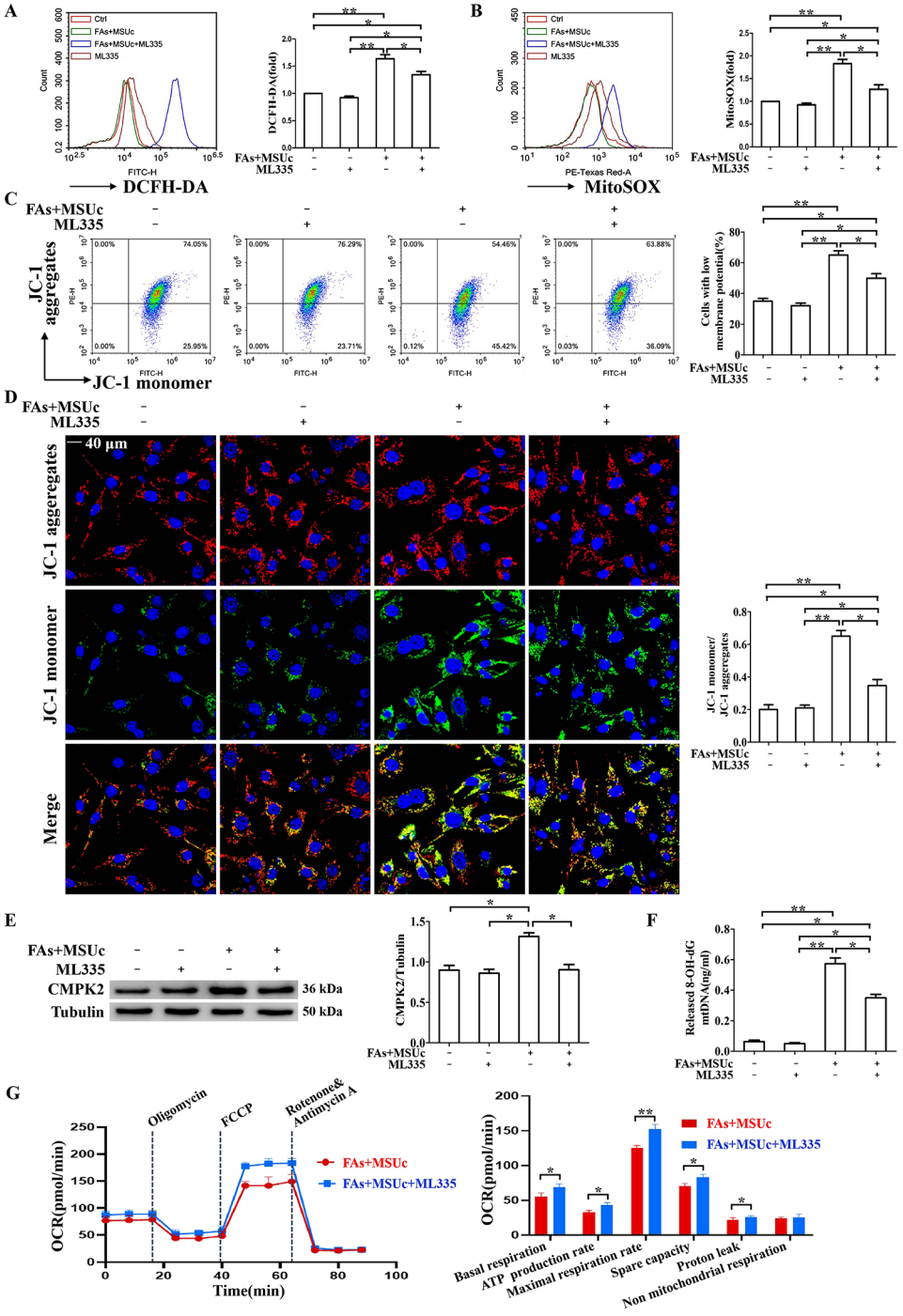

Fig. 2 ML335 treatment improved mitochondrial function and reduced mitochondrial DNA levels. (**A**) DCFH-DA probe staining and flow cytometry were used to detect intracellular total ROS. (**B**) MitoSOX probe staining and flow cytometry were used to detect mitochondrial ROS. (**C**, **D**) Mitochondrial membrane potential was respectively measured by flow cytometry and laser confocal microscope imaging after staining with the JC-1 probe. Hoechst33342 stains nuclei. Scale bar, 40 μm. (**E**) Western blotting was used to detect CMPK protein level in the lysates of BMDMs. (**F**) ELISA was used to detect oxidized mitochondrial DNA levels in the lysates of BMDMs. (**G**) Mitochondria respiration (oxygen consumption rate, OCR) was measured using Seahorse XFe24 Analyzer. Statistical analysis of basal respiration, ATP production, maximal respiration rate, spare capacity, proton leak, non mitochondrial respiration ($n = 5$ biological replicates)

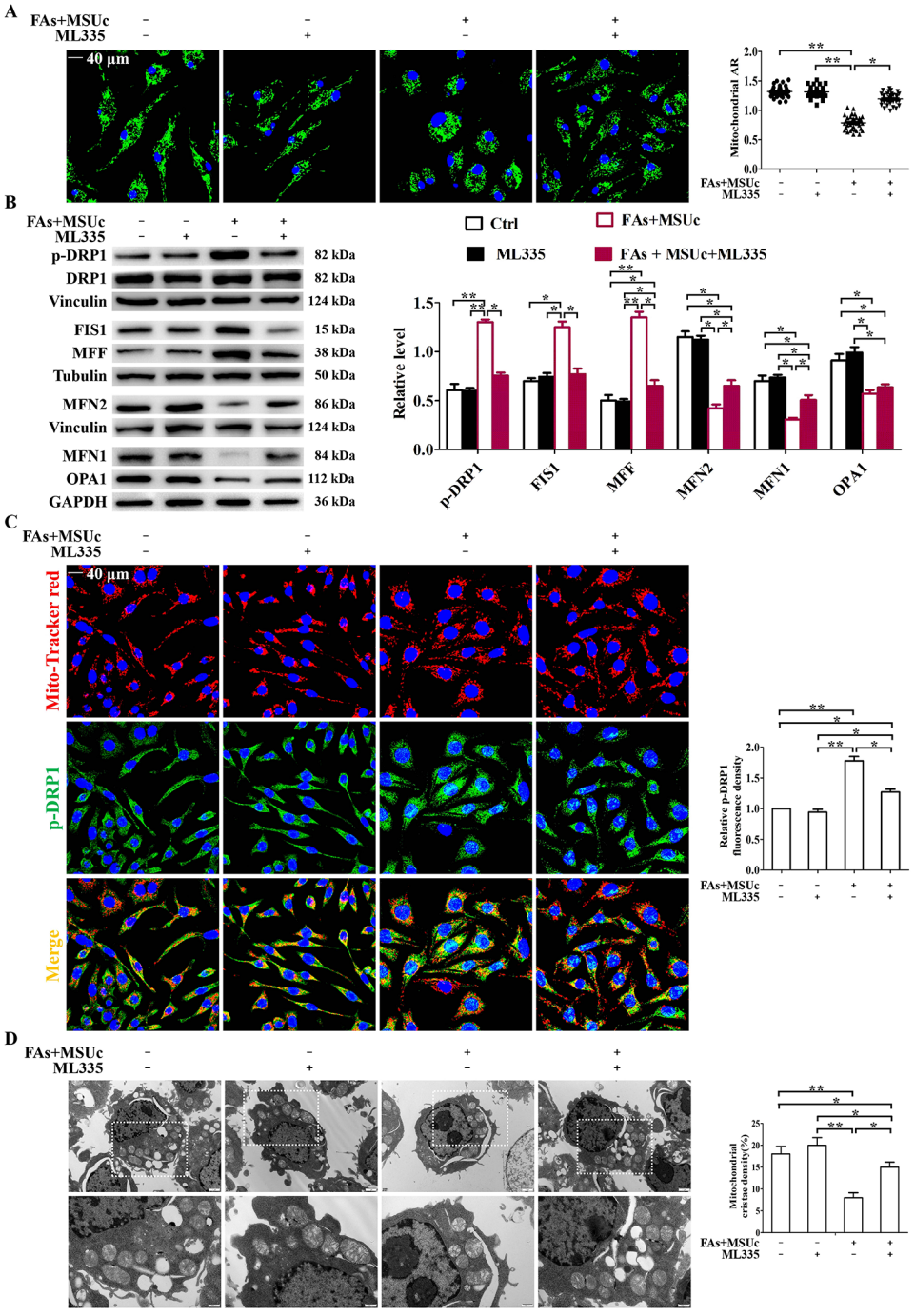

Fig. 3 ML335 accelerates mitochondrial dynamics homeostasis and mitochondrial ultrastructure. (**A**) Representative LCM imaging of Mito-Tracker green probe staining in live BMDMs, Hoechst33342 stains nuclei. Scale bar, 40 μm. (**B**) Western blotting was used to detect mitochondrial fission/fusion-related protein expression. The relative levels of p-DRP1/DRP1 (Vinculin as loading control), FIS1/Tubulin, MFF/Tubulin, MFN2/Vinculin, MFN1/GAPDH, OPA1/GAPDH were displayed on the right. (**C**) Representative LCM imaging of BMDMs co-stained with Mito-Tracker Red probe and p-DRP1 immunofluorescence, Hoechst33342 stains nuclei. Scale bar, 40 μm. (**D**) Representative TEM images of mitochondrial (white box) ultrastructure in BMDMs. Scale bar: 1 μm. Image is representative of 10 images/sample; $n = 3$ samples/condition

the mitochondrial inner membrane that provide the high surface area for oxidative phosphorylation (OXPHOS) to generate ATP. These data suggest that ML335 improves mitochondrial fission/fusion balance for optimal structure/shape and function.

ML335 upregulates Sirt3 expression by suppressing March5 expression

Protein acetylation in mitochondria usually disrupts mitochondrial integrity and function [25]. We wanted to determine the effect of ML335 on the mitochondrial protein acetylation in BMDMs treated with FAs+MSUc. ML335 decreased the acetylation of FAs+MSUc-induced mitochondrial proteins (Fig. 4A). Sirt3 is a protein deacetylase located predominantly in mitochondria [26]. We examined the impact of ML335 on the expression of Sirt3. ML335 had almost no effect on Sirt3 at the mRNA level (Fig. 4B) but accelerated Sirt3 expression at the protein level (Fig. 4C). SOD2 is a very important target protein for the deacetylation of Sirt3 [27]. The present study

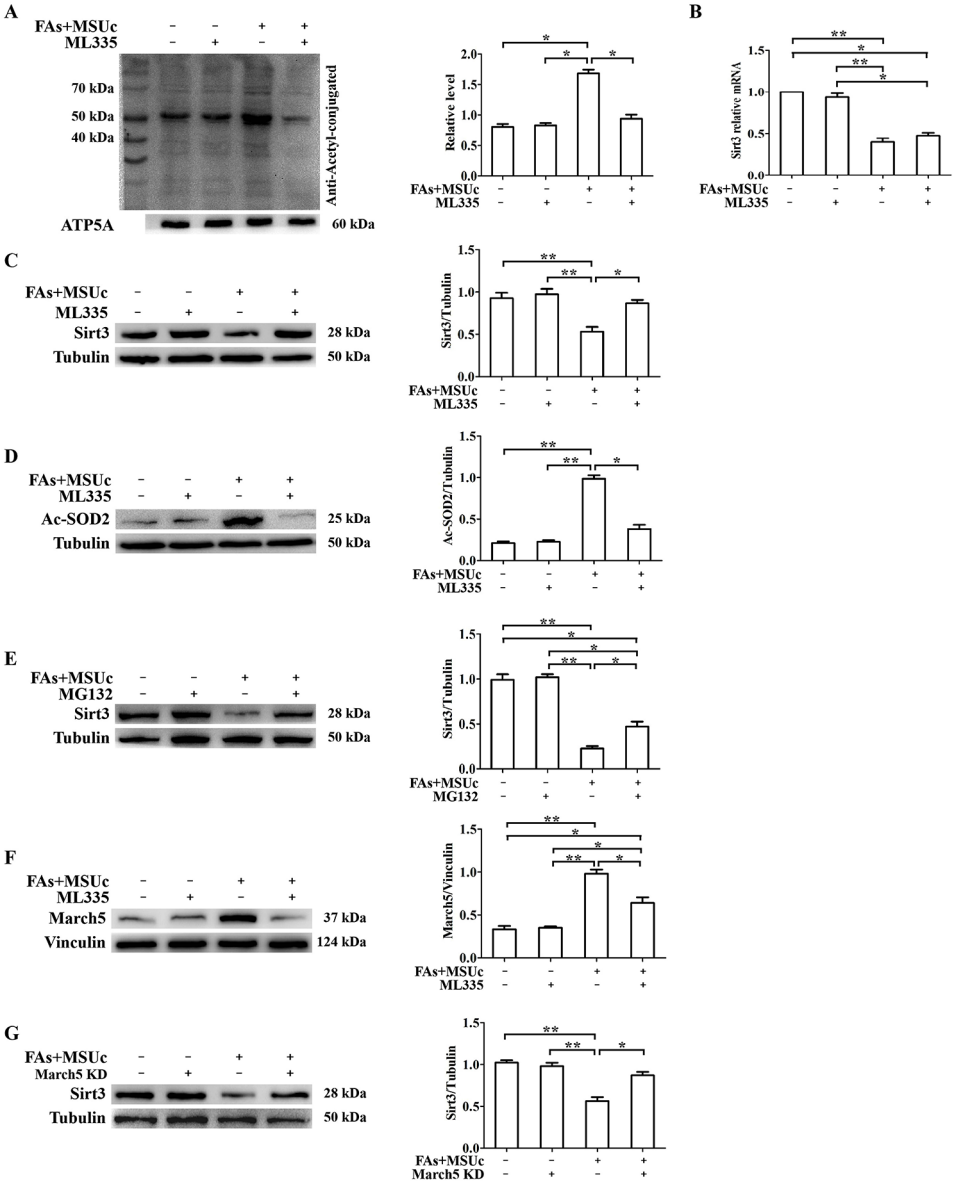

Fig. 4 ML335 promotes Sirt3 protein levels by inhibiting March5. (**A**) Western blotting was used to detect the effect of ML335 on acetylation levels of mitochondrial proteins with acetylated lysine antibodies. (**B**) RT-qPCR was used to detect the effect of ML335 on Sirt3 mRNA. (**C**) Western blotting was used to detect the effect of ML335 on Sirt3 protein level. (**D**) Western blotting was used to detect the effect of ML335 on acetylation of SOD2 protein in the lysates of BMDMs. (**E**) BMDMs were treated with FAs + MSUc for 8 h, then 10 μM MG132 was added for 4 h. Western blotting was used to detect Sirt3 protein level. (**F**) Western blotting was used to detect the effect of ML335 on March5 protein expression. (**G**) The effect of March5 knockdown (KD) on Sirt3 protein levels was detected by Western blotting

indicated that FAs+MSUc promoted the acetylation of SOD2 protein but inhibited SOD enzymatic activity in mitochondria, which was reversed by ML335 (Fig. 4D and Fig. S4A), suggesting that ML335 may moderate mitochondrial oxidative stress by promoting SOD activity.

The proteasomal inhibitor MG132 strongly blocked Sirt3 degradation induced by FAs+MSUc (Fig. 4E), suggesting that ML335 might affect ubiquitination of Sirt3 protein. MARCH5 (also known as MITOL) is an E3 ubiquitin ligase that promotes protein degradation in the mitochondria [28]. Our data showed that FAs+MSUc significantly stimulated the March5 protein level, but ML335 attenuated the March5 protein expression induced by FAs+MSUc (Fig. 4G). March5 knockdown inhibited the effect of FAs+MSUc on Sirt3 protein levels (Fig. 4H), while March5 overexpression reversed the upregulation of Sirt3 protein levels by ML335 (Fig. 5A). In accordance with this result, ML335 inhibited the ubiquitination of Sirt3 protein induced by FAs+MSUc (Fig. 5B and C). Overexpression of Sirt3 in BMDMs, IP data indicated that Sirt3 could interact with endogenous March5 protein (Fig. 5D). March5 overexpression in BMDMs, IP data showed that March5 could also interact with endogenous Sirt3 (Fig. 5E). These data suggested that there might be an interaction between endogenous March5 and Sirt3. Simultaneous overexpression of March5 and Sirt3 in BMDMs further demonstrated the existence of interaction between them (Fig. 5F). FAs+MSUc stimulation in BMDMs increased the interaction of Sirt3 with March5, while ML335 treatment blocked the March5 interaction with Sirt3 induced by FAs+MSUc (Fig. 5G). We further validated that ML335 suppressed FAs+MSUc-induced SIRT3 ubiquitination via inhibited March5 expression (Fig. S4B - S4D).

ML335 relieves mitochondrial dysfunction and inhibits mitochondrial fission by suppressing the expression of March5

Because ML335 affects Sirt3 protein levels via March5, we wanted to explore whether ML335 affects the acetylation of SOD2 protein through March5. March5 overexpression prevented the inhibition of SOD2 acetylation (Fig. 6A) and the promotion of mitochondrial SOD activity by ML335 (Fig. S4E). The next question we would like to resolve was whether ML335 was engaged in the regulation of mitochondrial dysfunction via March5. The study revealed that March5 overexpression prevented the protective effect of ML335 on mitochondrial dysfunction induced by MSU crystals, including mitochondrial ROS (Fig. 6B) and mitochondrial membrane potential (Fig. 6C).

Sirt3 is essential for maintaining LKB1 activity [29]. We examined the phosphorylation of LKB1 (p-LKB1, Ser428) in BMDMs treated with or without ML335 and found that ML335 promoted the phosphorylation of LKB1 (Fig. 6D). March5 overexpression decreased ML335-induced phosphorylation of LKB1 (Fig. 6E). LKB1 was identified as the key upstream kinase required for AMPK activation and mediates AMPK phosphorylation [30]. The data showed that ML335 dramatically increased the phosphorylation of AMPK (p-AMPK, Thr172) in BMDMs treated with FAs+MSUc (Fig. 6F). In addition, LKB1 knockdown hampered ML335-induced phosphorylation of AMPK (p-AMPK) in response to FAs+MSUc (Fig. 6G). It has been reported that AMPK affects the translocation of Drp1 by influencing the activity of downstream mitochondrial fission factor (MFF) [31]. This study showed that ML335 inhibited MFF expression (Fig. 6H) and Drp1 phosphorylation (Fig. 6I) and that inhibition of AMPK activity by compound C reversed the impact of ML335 on MFF protein expression (Fig. 6H) and p-Drp1 level (Fig. 6I). In addition, we also detected the effect of March5 knockdown on mitochondrial fusion proteins. Our study indicated that March5 knockdown promoted the expression of MFN1 and MFN2 but had little effect on the protein level of OPA1 (Fig. S5). These data imply that March5 has an essential function in regulating mitochondrial function and mitochondrial dynamics by ML335.

ML335 inhibits the proinflammatory phenotype shift of macrophages

To further assess how ML335 modulates the phenotypic switch of macrophages, we set up an IFN-γ+LPS/IL4-dependent BMDM activation model treated with or without ML335. The presence of ML335 was found to reduce the M1 population ($CD86^+$) induced by IFN-γ+LPS (Fig. 7A). We also observed an augmented IL-4-induced M2 population ($CD206^+$) in the presence of ML335 (Fig. 7B). Macrophages in acute gout are polarized toward the M1 phenotype at an early stage [32]. In BMDMs treated with FAs+MSUc, ML335 treatment attenuated the M1 population (Fig. 7C). In the present study, Western blotting data showed increased protein levels of M1 macrophage biomarkers such as CD86 and iNOS in response to FAs+MSUc (Fig. 7D). Protein expression of CD206, Arg1 and Arg2, biomarkers of the associated M2 phenotype, was greatly reduced because of FAs+MSUc stimulation (Fig. 7D). ML335 treatment downregulated M1 macrophage biomarker levels, but increased M2 macrophage biomarker levels (Fig. 7D). These data indicate that ML335 promotes the conversion of macrophages from an M1 pro-inflammatory phenotype to an M2 anti-inflammatory phenotype.

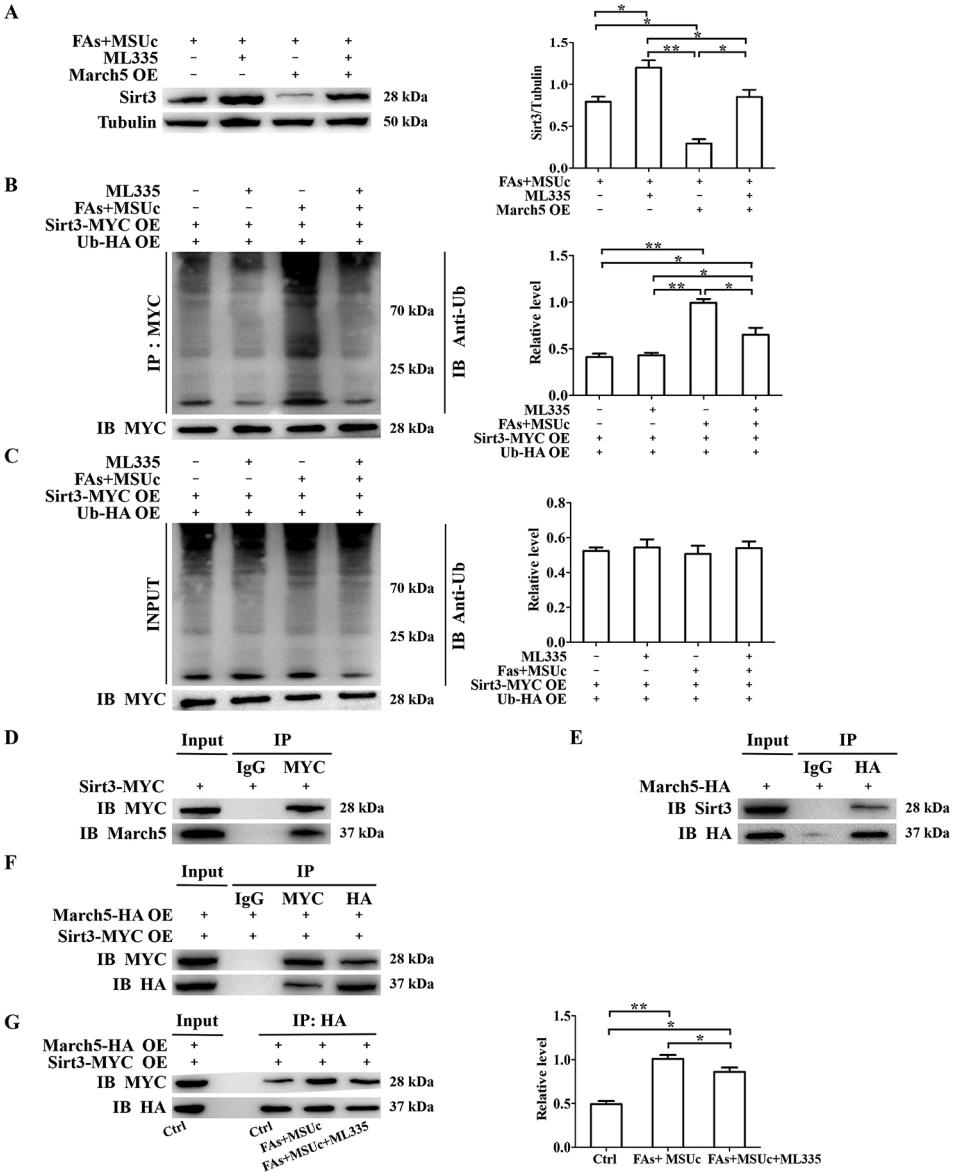

Fig. 5 ML335 inhibits Sirt3 ubiquitination and affects March5 interaction with Sirt3 protein. (**A**) Western blotting was used to detect the reverse effect of March5 overexpression on Sirt3 protein expression promoted by ML335. (**B, C**) BMDMs were transiently co-transfected with Sirt3-MYC and Ub-HA, and then treated with or without ML335 and FAs + MSUc. (**B**) IP was performed with anti-MYC antibody and the ubiquitination of Sirt3 was examined using the anti-ubiquitin anti-Ub after Western blotting. The relative level of ubiquitination of Sirt3 (Ub) /Sirt3 (MYC) was displayed on the right. (**C**) Ubiquitination of intracellular total protein was detected through Western blotting using anti-Ub. The relative level of ubiquitination of intracellular total proteins (Ub) /Sirt3 (MYC) was displayed on the right. (**D**) BMDMs were transiently transfected with Sirt3-MYC, IP was performed with MYC antibody, and the Sirt3 interaction with endogenous March5 detected through Western blotting using anti-March5. (**E**) BMDMs were transiently transfected with March5-HA, IP was performed with HA antibody, and the March5 interaction with endogenous Sirt3 was detected through Western blotting using anti-Sirt3. (**F**) BMDMs were transiently co-transfected with Sirt3-MYC and March5-HA, IP was performed with MYC or HA antibody, and the interaction between March5 and Sirt3 was detected through Western blotting using anti-MYC or anti-HA. (**G**) BMDMs were transiently co-transfected with Sirt3-MYC and March5-HA, treated with or without ML335 and FAs + MSUc, IP was performed with HA antibody, and the effect of ML335 on the interaction of March5 and Sirt3 induced by FAs + MSUc was detected through Western blotting using anti-MYC. The relative level of Sirt3 (MYC)/March5 (HA) was displayed on the right

ML335 ameliorates FAs + MSU crystal-induced macrophage metabolic defects

There is an intrinsic link between macrophage polarization and metabolic reprogramming. MSUc has been shown to affect lipid, carbohydrate, and amino acid metabolic pathways [33]. The protein levels of lipid metabolism-related genes, including fatty acid uptake (CD36) (Fig. 8A), fatty acid synthesis (FASN, p-ACC1) (Fig. 8B) and fatty acid oxidation (CPT1A, CPT-2, ACADL, HADH) (Fig. 8C), were significantly higher in BMDMs treated with FAs + MSUc than in the Ctrl group,

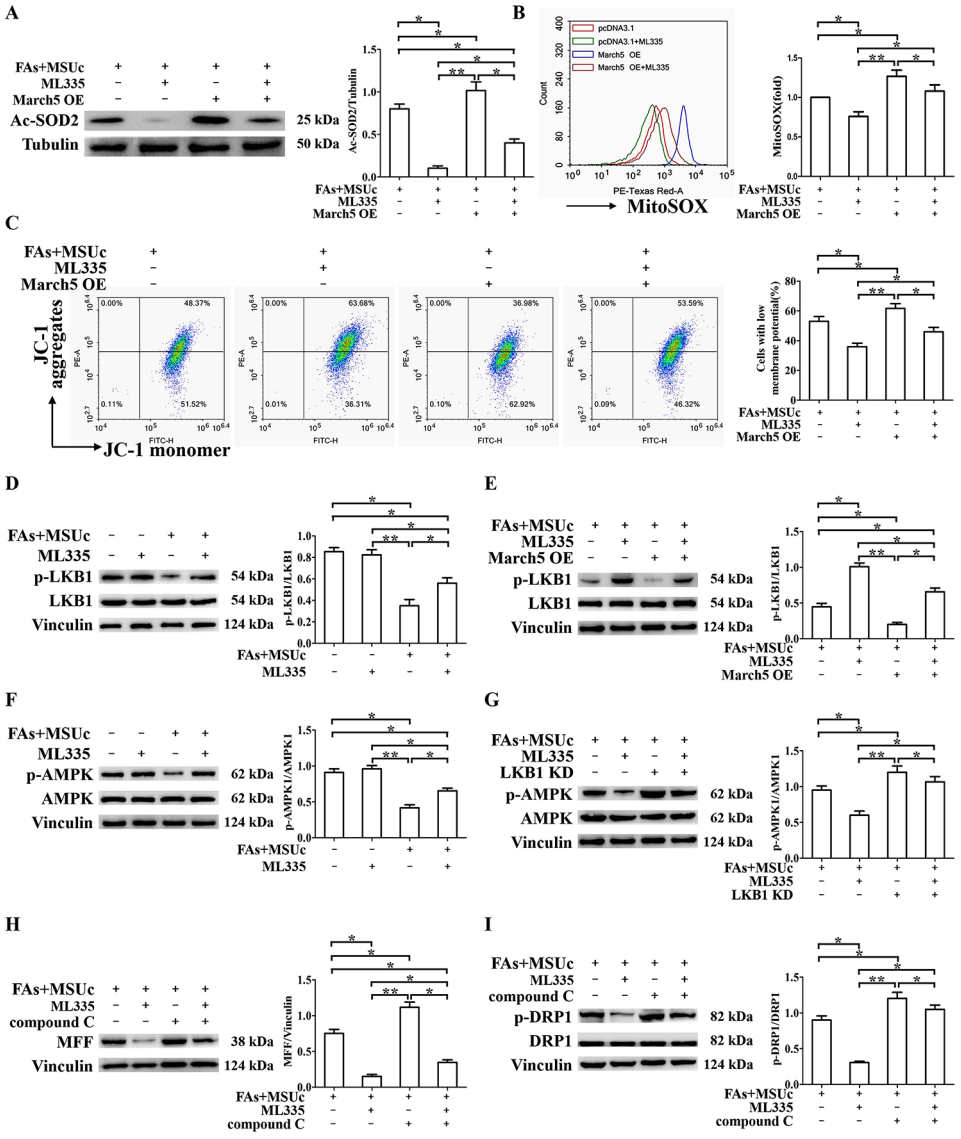

Fig. 6 ML335 attenuates mitochondrial dysfunction and suppresses mitochondrial fission via down-regulating March5. (**A**) Western blotting was used to detect the reverse effect of March5 overexpression on Ac-SOD2 protein expression inhibited by ML335. (**B**) MitoSOX probe staining and flow cytometry assay were used to detect mitochondrial ROS. The relative level of MitoSOX was displayed on the right. (**C**) Mitochondrial membrane potential was measured by flow cytometry after staining with the JC-1 probe. Statistical analyses of the proportion of cells with low mitochondrial membrane potential are shown on the right. (**D**) Western blotting was used to detect the effect of ML335 on p-LKB1 and LKB1 protein levels. The relative level of p-LKB1/LKB1 (Vinculin as loading control) was displayed on the right. (**E**) March5 overexpression prevented the up-regulation of p-LKB1 by ML335 as detected by Western blotting. The relative level of p-LKB1/LKB1 (Vinculin as loading control) was displayed on the right. (**F**) The effect of ML335 on p-AMPK detected by Western blotting. The relative level of p-AMPK/AMPK (Vinculin as loading control) was displayed on the right. (**G**) LKB1 knockdown prevented the upregulation of p-AMPK protein by ML336 as detected by Western blotting. The relative level of p-AMPK/AMPK (Vinculin as loading control) was displayed on the right. (**H**, **I**) Compound C reversed the down-regulation of MFF and p-DRP1 by ML335 as detected by Western blotting. The relative level of p-AMPK/AMPK (Vinculin as loading control) was displayed on the right

suggesting that the fatty acid oxidation (FAO) metabolic pathway was enhanced in FAs+MSUc-induced inflammation. ML335 markedly reduced the expression of these lipid metabolism-associated proteins induced by FAs+MSUc (Fig. 8A and C). We further investigated the impact of ML335 on metabolites in BMDMs treated with FAs+MSUc. In total, 245 metabolites were detected with the T500 untargeted metabolomics assay. There were 77 metabolites that were statistically different between FAs+MSUc vs. FAs+MSUc+ML335. Of these, 12 metabolites were downregulated, and 65 metabolites were upregulated. The KEGG enrichment indicated that ML335 has a strong influence on metabolic pathways (Fig. S6). As shown by the heatmap of metabolomics, ML335 mainly had an effect on the following four classes of metabolites: carnitine (CAR), amino acids, nucleotides

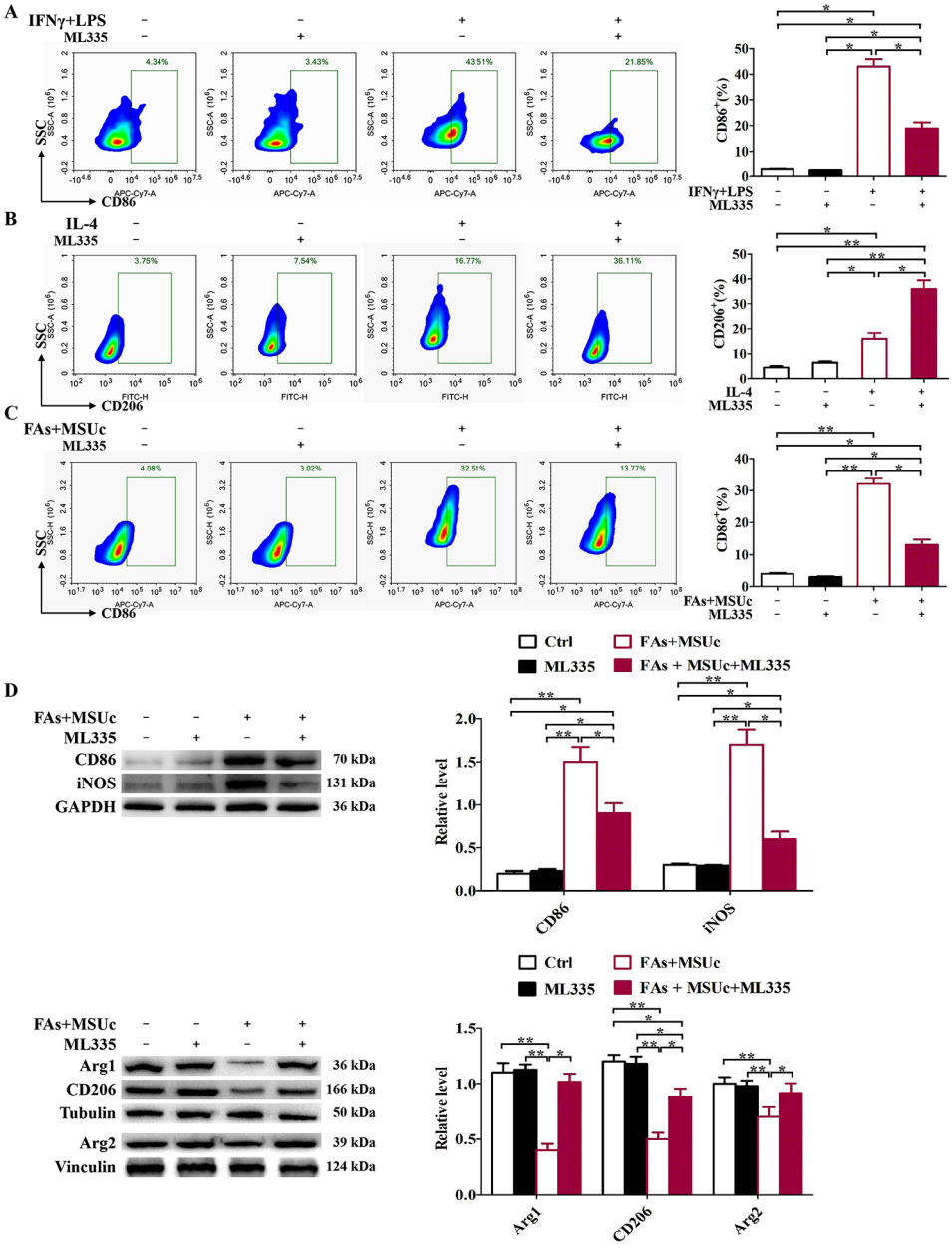

Fig. 7 ML335 inhibits the pro-inflammatory phenotype shift of macrophages (**A**) Flow cytometry analysis of the effect of ML335 on M1 populations ($CD86^+$) in BMDMs treated with IFNγ + LPS. (**B**) Flow cytometry detection of the effect of ML335 on M2 population ($CD206^+$) in BMDMs treated with IL-4. (**C**) Effect of ML335 on FAs + MSUc-induced M1 population was detected by flow cytometry ($CD86^+$). (**D**) Western blotting was used to detect CD86, iNOS, Arg1, CD206 and Arg2 protein expression. Histograms represent statistical analyses of data from three independent experiments on the right

and their metabolomics, organic acids and their derivatives (Fig. S7). Acylcarnitine levels are closely related to FAO. ML335 not only increased short-chain acylcarnitine levels (DL-carnitine, acetyl-carnitine, isovaleryl-carnitine and 2-methylbutyroylcarnitine) but also long-chain acylcarnitines (L-palmitoylcarnitine) in BMDMs treated with FAs + MSUc (Fig. 8D). However, ML335 decreased the ratio of L-palmitoylcarnitine to DL-carnitine induced by FAs + MSUc (Fig. 8E), suggesting that ML335 inhibited the activity of FAO. Lysine and methionine are the precursors for carnitine biosynthesis, and our data indicated that ML335 upregulated the levels of lysine and L-methionine (Fig. 8D). We further analyzed the effect of ML335 on urea cycle-related metabolites. ML335 increased the levels of ornithine, L-aspartate, argininosuccinic acid, fumaric acid and arginine but had little effect on the levels of L-citrulline and increased the ratio of ornithine to arginine (Fig. 8D and F). Based on the association of serine and glycine with macrophage polarity, we analyzed the effect of ML335 on serine and glycine

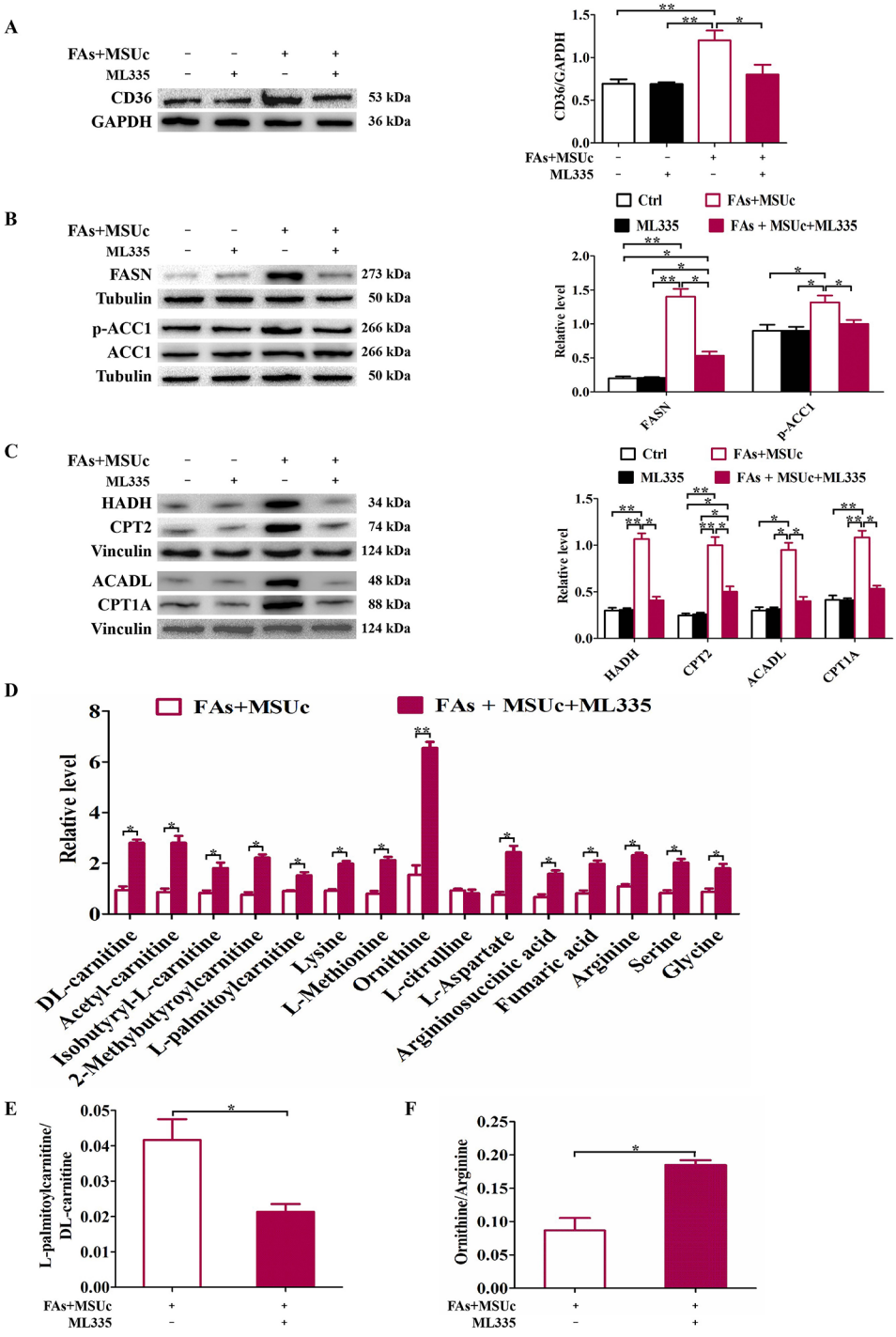

Fig. 8 ML335 ameliorates macrophage metabolic defects induced by FAs + MSUc. (**A**) Representative images of Western blotting and quantitative analysis of CD36. (**B**) Representative images of Western blotting for FASN, p-ACC1 and ACC1. The relative levels of FASN/ Tubulin, p-ACC1/ACC1 (Tubulin as loading control) were displayed on the right. (**C**) Representative images of Western blotting and quantitative analysis of HADH, CPT2, ACADL and CPT1A. (**D**) Statistical analysis of the metabolites DL-carnitine, Acetyl-carnitine, Isobutyryl-L-carnitine, 2-Methybytyroylcarnitine, L-palmitoylcarnitine, Lysine, L-Methionine, Ornithine, L-citrulline, L-Aspartate, Argininosuccinic acid, Fumaric acid, Arginine, Serine and Glycine. (**E**) Statistical analysis of the ratio of L-palmitoylcarnitine to DL-carnitine. (**F**) Statistical analysis of the ratio of Ornithine to Arginine

levels. ML335 promoted the levels of serine and glycine in BMDMs treated with FAs+MSUc (Fig. 8D). All these data suggest that ML335 restores the metabolic defects induced by FAs+MSUc.

ML335 alleviated MSU crystal-induced paw swelling and peritonitis model in mice

To investigate the anti-inflammatory function of ML335 in vivo, the MSU crystal-induced mouse paw swelling and peritonitis model were treated with ML335. In MSU crystal-injected mice treated with ML335, a remarkable reduction in the swelling index of the paw was observed (Fig. 9A). In addition, inflammatory cells in paw sections were detected by HE staining, and the infiltration of inflammatory cells was significantly decreased in MSU crystal-injected mice after ML335 treatment (Fig. 9B). Immunofluorescence staining showed that ML335 treatment inhibited the distribution of CD11b and MPO positive cells in tissue sections of paws injected with MSU crystals (Fig. S8A). Meanwhile, ML335 treatment inhibited the protein levels of KCNK6, MPO and p-DRP1, while promoted the protein expression of p-AMPK in the tissues of MSU crystal-injected paws (Fig. 9C). We further assessed the effects of ML335 on the migration of inflammatory cells and cytokine secretion in a model of peritonitis induced by MSU crystals. ML335 blunted peritonitis induced by MSU crystals, as demonstrated by a reduction in leukocyte ($CD45^+$), neutrophil ($Ly6G^+$), and macrophage (F4/80) counts (Fig. 9D), as well as decreased secretion of cytokines IL-1β, CCL2 and IL-6 in the peritoneal lavage fluid (Fig. S8B).

Discussion

It is widely recognized that potassium efflux is sufficient and necessary for activation of the NLRP3 inflammasome in most cases [8, 13, 34, 35]. TWIK2 channels may be promising drug targets for the treatment of NLRP3 inflammation-related diseases. We assayed the impact of five known K2P channel modulators on the secretion of IL-1β in MSU crystal-stimulated macrophages. All five compounds inhibited the secretion of IL-1β induced by FAs+MSUc, but the lowest level of IL-1β secretion was observed in macrophages after ML335 treatment. Disruption of ion homeostasis affects the level of mitochondrial ROS and is the upstream signal for activation of the NLRP3 inflammasome [36]. Increasing evidence suggests that oxidative stress and mitochondrial dysfunction contribute to the MSU crystal-induced inflammatory response [37–40]. Mitochondria have essential functions in regulating a variety of metabolic processes, ATP production, and maintenance of cellular redox homeostasis. In our study, we found that ML335 effectively increased intracellular K^+ concentraion, improved mitochondrial function and inhibited NLRP3 inflammasome activation. KCNK6 overexpression dramatically impaired the inhibitory effect of ML335 on intracellular potassium efflux and IL-1β secretion induced by FAs+MSUc, implying that ML335 might block FAs+MSUc-induced NLRP3 inflammasome activation mainly by inhibiting KCNK6 activity.

Dysregulation of mitochondrial dynamics can directly affect mitochondrial function and result in pathological conditions [41]. The mitochondrial inner and outer membrane fusion family acts in mitochondrial fusion, with MFN1 and MFN2 localised in the mitochondrial outer membrane and mediating outer membrane fusion. OPA1 localised in the mitochondrial inner membrane, mediating inner membrane fusion [42]. Phosphorylation of Drp1(Drp1s616) drives mitochondrial fission [43], and Drp1 is recruited from the cytoplasm to the outer mitochondrial membrane by interacting with other mitochondrial fission proteins, including mitochondrial fission factor (MFF) and fission protein 1 (Fis1) [44, 45]. MFF recruits Drp1 to translocate to mitochondria and affects mitochondrial fission [46]. Phosphorylation of serine at site 616 of DRP1 promotes DRP1 activity, which stimulates DRP1 translocation to mitochondria and accelerates fission [47]. Our current study found that ML335 treatment upregulated the expression of mitochondrial fusion proteins MFN1 and MFN2, inhibited the level of phosphorylated Drp1 (s616) and, in particular, blocked the mitochondrial translocation of DRP1. These data suggest a protective effect of ML335 on mitochondrial dynamics.

The function of MITOL (March5) in shaping mitochondrial dynamics is still controversial. MITOL has been reported to interact with Drp1, resulting in its proteasome-dependent degradation and ubiquitination, thereby suppressing mitochondrial hyperfission [28, 48]. Nevertheless, it has been noted that MITOL has the opposite effect on mitochondrial fission [49]. Karbowski's group reported that MITOL ubiquitinates the Drp1 receptor Mid49, degrading it and thereby controlling mitochondrial fission [50]. These observations indicate that there may be some specificity in MITOL's regulation of its substrates, particularly Drp1. MITOL can also ubiquitinate MFN1 or MFN2, resulting in protein degradation [51, 52]. SIRT3 is an important metabolic sensor related to mitochondrial homeostasis and is also involved in regulating mitochondrial dynamics remodeling [53, 54]. Despite the localization of March5 to the outer mitochondrial membrane and SIRT3 to the mitochondrial matrix, our study indicated that March5 is able to interact with SIRT3 and can regulate the ubiquitination of SIRT3 protein. SIRT3 is encoded by a nuclear gene, and we hypothesized that SIRT3 might interact with MARCH5 during its translocation from the outer mitochondrial membrane to the mitochondrial matrix. This study revealed that ML335 can effectively

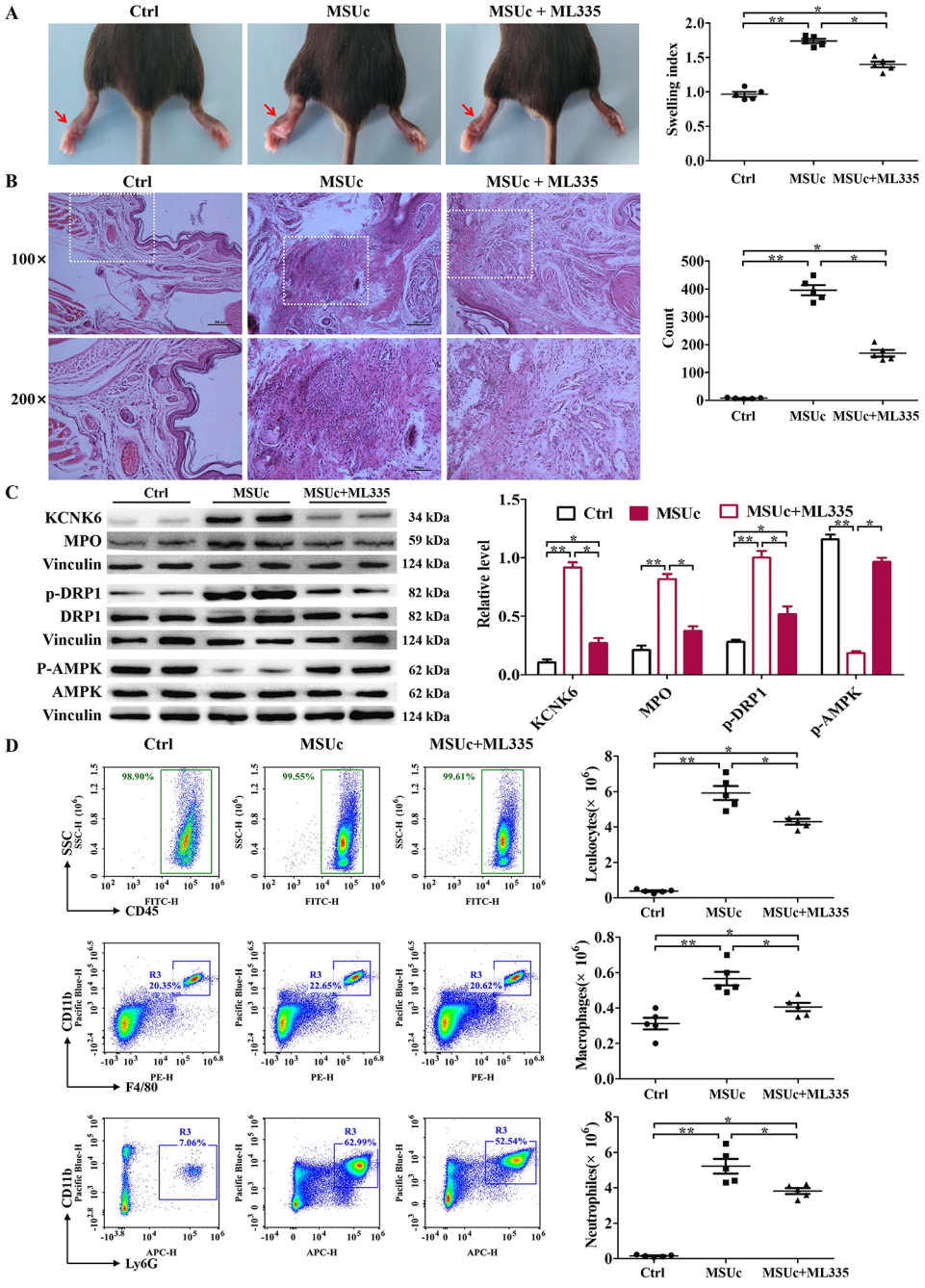

Fig. 9 ML335 inhibited the inflammatory response in MSU crystal-induced paw swelling and peritonitis of mouse models. (**A**) The paw thickness of mice and statistical analysis of paw swelling index. (**B**) Representative microscopic images of mouse paw sections stained with hematoxylin-eosin (HE) (magnification 10 × 10 and 20 × 10). (**C**) Representative image of Western blotting and quantitative analyses of p-DRP1, KCNK6, MPO, p-AMPK. The relative levels of KCNK6/Vinculin, MPO/Vinculin, p-DRP1/DRP1 (Vinculin as loading control), p-AMPK/AMPK (Vinculin as loading control) were depicted on the right. (**D**) Representative plots of migrated leukocytes ($CD45^+$), macrophages ($CD11b^+$ $F4/80^+$) and neutrophils ($CD11b^+$ $Ly6G^+$) in peritoneal fluid were detected by flow cytometry analysis. The number of migrated leukocytes, macrophages and neutrophils were quantified and compared among the groups on the right. $n = 6$ mice for each group

inhibit the ubiquitination of MSU crystal-induced SIRT3 protien. ML335 inhibits the degradation of Sirt3 by suppressing the expression of March5 and further attenuates the phosphorylation level of Drp1 (s616) through SIRT3/LKB1/AMPK signaling. In addition, March5 overexpression reversed the impact of ML335 on mitochondrial ROS and mitochondrial membrane potential. In the present study, we reveal a novel mechanism by which ML335 can ameliorate FA + MSU crystal-induced

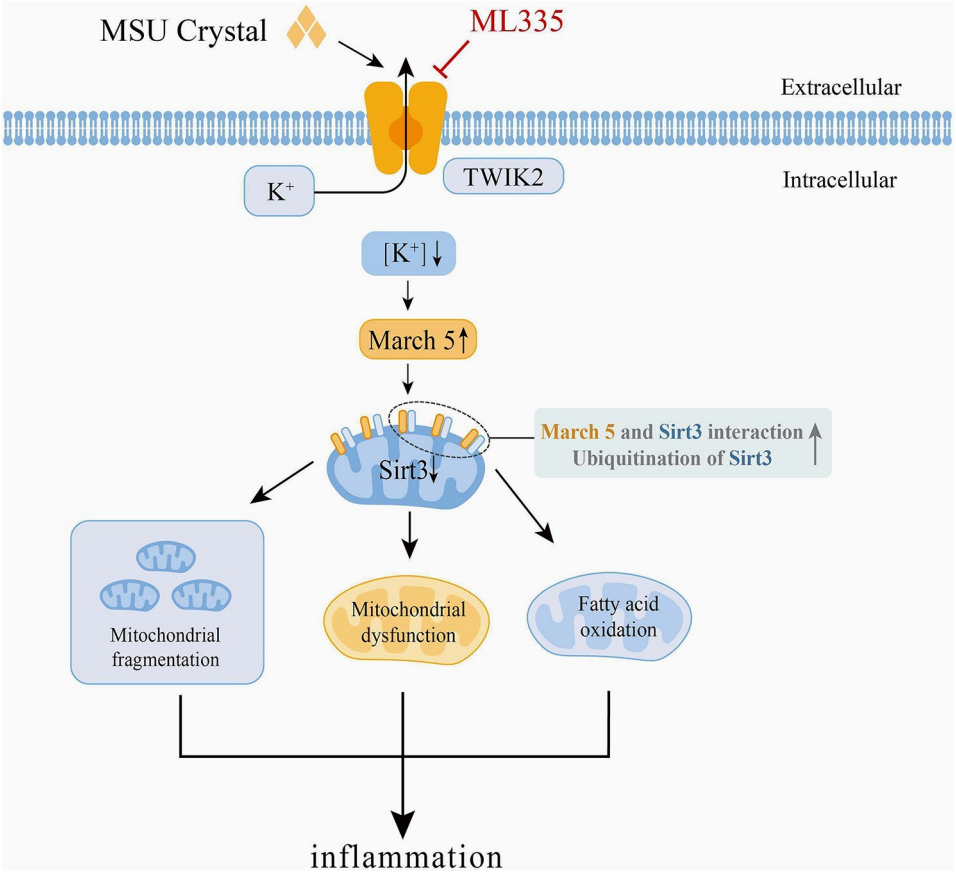

Fig. 10 ML335 inhibits TWIK2 channel-mediated potassium efflux and attenuates mitochondrial damage in MSU crystal-induced inflammation. ML335 upregulates intracellular potassium concentration by inhibiting the activity of the MSU crystal-triggered potassium efflux channel TWIK2. ML335 also blocks the interaction between March5 and Sirt3, thereby decreasing the ubiquitination of Sirt3 protein, while maintaining mitochondrial dynamic homeostasis and alleviating mitochondrial dysfunction and metabolic defects

mitochondrial fragmentation and functional damage by inhibiting March5 expression.

Alterations in macrophage polarization were observed in all phases of gout inflammation. The infiltration of M1 macrophages was positively related to arthritis severity [32]. NLRP3 inflammasome activation plays an essential role in various inflammatory diseases by regulating macrophage M1 polarization [55]. Drp1-mediated mitochondrial fragmentation is associated with NLRP3 inflammasome activation [55, 56]. Inhibition of DRP1-dependent mitochondrial fission regulates M1 polarization [55]. This study confirmed that ML335 decreased both Drp1 activity and NLRP3 inflammasome activation. More importantly, ML335 suppressed M1-related biomarker expression and M1 population. These data strongly indicate that ML335 is involved in the modulation of macrophage activation.

Metabolic reprogramming often occurs during macrophage activation and affects macrophage polarization. Sirt3 regulates metabolic processes, including FAO, oxidative phosphorylation, the urea cycle and the antioxidant response in mitochondria [57]. It has been shown that fatty acid oxidation promotes macrophage activation in gout inflammation [11]. Recently, it has been reported that genes upregulated upon MSUc stimulation of macrophages mainly include lipid and amino acid metabolism, glycolysis, and SLC transporters [33]. In this study, ML335 treatment led to the upregulation of 15 amino acids. Of these 15 amino acids, our previous metabolomics data revealed that FA+MSUc stimulation barely affected the levels of lysine, threonine, glycine, and glutamate but decreased the levels of the remaining 11 amino acids. A recent study reported that alanine and aspartate showed significant differences between frequent versus infrequent gout flares [58]. Enhanced amino acid uptake occurs in macrophages with anti-inflammatory properties. In line with previous reports, ML335 inhibited macrophage activation and simultaneously promoted intracellular amino acid levels.

In conclusion, our study demonstrates that ML335 relieves FA+MSUc-induced inflammation in vivo and in vitro. ML335 can accelerate the expression of SIRT3 by inhibiting March5 expression, which is accompanied by maintaining mitochondrial dynamic homeostasis,

reducing oxidative stress and increasing energy production (Fig. 10). This study highlights the potential value of ML335 in the treatment of gout.

Supplementary Information

The online version contains supplementary material available at https://doi.org/10.1186/s12967-024-05303-7.

Supplementary Material 1

Author contributions

DZS performed all aspects of this study, XQZ and QQY performed experiments and analyzed the data. RJL provided critical reagents and technical advice. QD and MZ organized the study and prepared the manuscript. All authors read the manuscript and provided comments.

Funding

This research was supported by grants (No. 81972119) from the National Natural Science Foundation of China; the Sichuan Province Science and Technology Support Project (22NSFSC0781 and 2023ZYD0060); and the Nanchong City Science and Technology Support Project (19SXHZ0456 22SXQT0372 and 21YFZJ0099).

Data availability

Data will be made available on request.

Declarations

Ethics approval

The animal experiments were approved by the Institutional Animal Care and Use Committee of North Sichuan Medical College (202155).

Competing interest

All listed authors of this manuscript have approved of the manuscript to submit to Pharmacological Research including its copyright transfer at acceptance for publication. The authors declare that there is no conflict of interest associated with this manuscript.

Author details

[1]Institute of Rheumatology and Immunology, The Affiliated Hospital of North Sichuan Medical College and Institute of Basic Medicine and Forensic Medicine, North Sichuan Medical College, Nanchong 637001, Sichuan, China
[2]Medical Imaging Key Laboratory of Sichuan Province, North Sichuan Medical College, Nanchong 637001, Sichuan, China
[3]North Sichuan Medical College Innovation Centre for Science and Technology, North Sichuan Medical College, Nanchong 637001, Sichuan, China

Received: 8 August 2023 / Accepted: 22 October 2023
Published online: 22 August 2024

References

1. Rai SK, Avina-Zubieta JA, McCormick N, De Vera MA, Shojania K, Sayre EC, Choi HK. The rising prevalence and incidence of gout in British Columbia, Canada: Population-based trends from 2000 to 2012. Semin Arthritis Rheum. 2017;46(4):451–6.
2. Chen Y, Tang Z, Huang Z, Zhou W, Li Z, Li X, Sun F. The prevalence of gout in mainland China from 2000 to 2016: a systematic review and meta-analysis. J Public Health. 2017;25(5):521–9.
3. Dalbeth N, Gosling AL, Gaffo A, Abhishek A. Gout Lancet. 2021;397(10287):1843–55.
4. Qaseem A, Harris RP, Forciea MA, Clinical Guidelines Committee of the American College of P, Denberg TD, Barry MJ, Boyd C, Chow RD, Humphrey LL, Kansagara D, Vijan S, Wilt TJ. Management of Acute and recurrent gout: a clinical practice Guideline from the American College of Physicians. Ann Intern Med. 2017;166(1):58–68.
5. Pascart T, Liote F. Gout: state of the art after a decade of developments. Rheumatology (Oxford). 2019;58(1):27–44.
6. Lee JS, Kwon OC, Oh JS, Kim YG, Lee CK, Yoo B, Hong S. Clinical features and recurrent attack in gout patients according to serum urate levels during an acute attack. Korean J Intern Med. 2020;35(1):240–8.
7. Leung YY, Yao Hui LL, Kraus VB. Colchicine–update on mechanisms of action and therapeutic uses. Semin Arthritis Rheum. 2015;45(3):341–50.
8. Gong T, Yang Y, Jin T, Jiang W, Zhou R. Orchestration of NLRP3 inflammasome activation by Ion Fluxes. Trends Immunol. 2018;39(5):393–406.
9. Lin Y, Luo T, Weng A, Huang X, Yao Y, Fu Z, Li Y, Liu A, Li X, Chen D, Pan H. Gallic acid alleviates gouty arthritis by inhibiting NLRP3 inflammasome activation and pyroptosis through enhancing Nrf2 signaling. Front Immunol. 2020;11:580593.
10. Hsieh CY, Li LH, Rao YK, Ju TC, Nai YS, Chen YW, Hua KF. Mechanistic insight into the attenuation of gouty inflammation by Taiwanese green propolis via inhibition of the NLRP3 inflammasome. J Cell Physiol. 2019;234(4):4081–94.
11. Hall CJ, Sanderson LE, Lawrence LM, Pool B, van der Kroef M, Ashimbayeva E, Britto D, Harper JL, Lieschke GJ, Astin JW, Crosier KE, Dalbeth N, Crosier PS. Blocking fatty acid-fueled mROS production within macrophages alleviates acute gouty inflammation. J Clin Invest. 2018;128(5):1752–71.
12. Yang G, Lee HE, Moon SJ, Ko KM, Koh JH, Seok JK, Min JK, Heo TH, Kang HC, Cho YY, Lee HS, Fitzgerald KA, Lee JY. Direct binding to NLRP3 pyrin domain as a novel strategy to prevent NLRP3-Driven inflammation and gouty arthritis. Arthritis Rheumatol. 2020;72(7):1192–202.
13. Munoz-Planillo R, Kuffa P, Martinez-Colon G, Smith BL, Rajendiran TM, Nunez G. K + efflux is the common trigger of NLRP3 inflammasome activation by bacterial toxins and particulate matter. Immunity. 2013;38(6):1142–53.
14. Petrilli V, Papin S, Dostert C, Mayor A, Martinon F, Tschopp J. Activation of the NALP3 inflammasome is triggered by low intracellular potassium concentration. Cell Death Differ. 2007;14(9):1583–9.
15. Xu Z, Chen ZM, Wu X, Zhang L, Cao Y, Zhou P. Distinct molecular mechanisms underlying potassium efflux for NLRP3 inflammasome activation. Front Immunol. 2020;11:609441.
16. Pelegrin P, Surprenant A. The P2X(7) receptor-pannexin connection to dye uptake and IL-1beta release. Purinergic Signal. 2009;5(2):129–37.
17. Di Virgilio F, Dal Ben D, Sarti AC, Giuliani AL, Falzoni S. The P2X7 receptor in infection and inflammation. Immunity. 2017;47(1):15–31.
18. Di AK, Xiong SQ, Ye ZM, Malireddi RKS, Kometani S, Zhong M, Mittal M, Hong ZG, Kanneganti TD, Rehman J, Malik AB. The TWIK2 potassium efflux channel in macrophages mediates NLRP3 inflammasome-induced inflammation. Immunity. 2018;49(1):56–.
19. Enyedi P, Czirjak G. Molecular background of Leak K + currents: two-pore Domain Potassium channels. Physiol Rev. 2010;90(2):559–605.
20. Huang LS, Anas M, Xu JS, Zhou BS, Toth PT, Krishnan Y, Di AK, Malik AB, Vanaja S. Endosomal trafficking of two-pore K + efflux channel TWIK2 to plasmalemma mediates NLRP3 inflammasome activation and inflammatory injury. Elife. 2023;12.
21. Wang YQ, Wang C, He QL, Chen GN, Yu J, Cang J, Zhong M. Inhibition of sphingosine-1-phosphate receptor 3 suppresses ATP-induced NLRP3 inflammasome activation in macrophages via TWIK2-mediated potassium efflux. Front Immunol. 2023;14.
22. Wu XY, Lv JY, Zhang SQ, Yi X, Xu ZW, Zhi YX, Zhao BX, Pang JX, Yung KKL, Liu SW, Zhou PZ. ML365 inhibits TWIK2 channel to block ATP-induced NLRP3 inflammasome. Acta Pharmacol Sin. 2022;43(4):992–1000.
23. Chen BF, Li HM, Ou GC, Ren L, Yang XH, Zeng M. Curcumin attenuates MSU crystal-induced inflammation by inhibiting the degradation of I kappa B alpha and blocking mitochondrial damage. Arthritis Res Ther. 2019;21(1).
24. McWherter C, Choi YJ, Serrano RL, Mahata SK, Terkeltaub R, Liu-Bryan R. Arhalofenate acid inhibits monosodium urate crystal-induced inflammatory responses through activation of AMP-activated protein kinase (AMPK) signaling. Arthritis Res Ther. 2018;20.
25. Baeza J, Smallegan MJ, Denu JM. Mechanisms and Dynamics of Protein Acetylation in Mitochondria. Trends Biochem Sci. 2016;41(3):231–44.
26. Kincaid B, Bossy-Wetzel E. Forever young: SIRT3 a shield against mitochondrial meltdown, aging, and neurodegeneration. Front Aging Neurosci. 2013;5:48.
27. Ansari A, Rahman MS, Saha SK, Saikot FK, Deep A, Kim KH. Function of the SIRT3 mitochondrial deacetylase in cellular physiology, cancer, and neurodegenerative disease. Aging Cell. 2017;16(1):4–16.

28. Nakamura N, Kimura Y, Tokuda M, Honda S, Hirose S. MARCH-V is a novel mitofusin 2- and Drp1-binding protein able to change mitochondrial morphology. EMBO Rep. 2006;7(10):1019–22.
29. Zhang T, Liu J, Shen S, Tong Q, Ma X, Lin L. SIRT3 promotes lipophagy and chaperon-mediated autophagy to protect hepatocytes against lipotoxicity. Cell Death Differ. 2020;27(1):329–44.
30. Shaw RJ, Kosmatka M, Bardeesy N, Hurley RL, Witters LA, DePinho RA, Cantley LC. The tumor suppressor LKB1 kinase directly activates AMP-activated kinase and regulates apoptosis in response to energy stress. Proc Natl Acad Sci U S A. 2004;101(10):3329–35.
31. Li ZY, Lu GQ, Lu J, Wang PX, Zhang XL, Zou Y, Liu PQ. SZC-6, a small-molecule activator of SIRT3, attenuates cardiac hypertrophy in mice. Acta Pharmacol Sin. 2023;44(3):546–60.
32. Zhao L, Ye W, Zhu Y, Chen F, Wang Q, Lv X, Hua Y, Du Z, Zhu X, Yu Y, Zou H, Liu L, Xue Y. Distinct macrophage polarization in acute and chronic gout. Lab Invest. 2022;102(10):1054–63.
33. Cobo I, Cheng A, Murillo-Saich J, Coras R, Torres A, Abe Y, Lana AJ, Schlachetzki J, Liu-Bryan R, Terkeltaub R, Sanchez-Lopez E, Glass CK, Guma M. Monosodium urate crystals regulate a unique JNK-dependent macrophage metabolic and inflammatory response. Cell Rep. 2022;38(10):110489.
34. Walev I, Reske K, Palmer M, Valeva A, Bhakdi S. Potassium-inhibited processing of IL-1 beta in human monocytes. EMBO J. 1995;14(8):1607–14.
35. Hafner-Bratkovic I, Pelegrin P. Ion homeostasis and ion channels in NLRP3 inflammasome activation and regulation. Curr Opin Immunol. 2018;52:8–17.
36. Weinberg SE, Sena LA, Chandel NS. Mitochondria in the regulation of Innate and adaptive immunity. Immunity. 2015;42(3):406–17.
37. Chen SY, Li YP, You YP, Zhang HR, Shi ZJ, Liang QQ, Yuan T, Xu R, Xu LH, Zha QB, Ou-Yang DY, He XH. Theaflavin mitigates acute gouty peritonitis and septic organ injury in mice by suppressing NLRP3 inflammasome assembly. Acta Pharmacol Sin. 2023.
38. Castelblanco M, Lugrin J, Ehirchiou D, Nasi S, Ishii I, So A, Martinon F, Busso N. Hydrogen sulfide inhibits NLRP3 inflammasome activation and reduces cytokine production both in vitro and in a mouse model of inflammation. J Biol Chem. 2018;293(7):2546–57.
39. Zhou Y, Chen YJ, Zhong XW, Xia HT, Zhao MC, Zhao MY, Xu L, Guo XL, You CG. Lipoxin A4 attenuates MSU-crystal-induced NLRP3 inflammasome activation through suppressing Nrf2 thereby increasing TXNRD2. Front Immunol. 2022;13.
40. Zhao L, Zhao TY, Yang X, Cao L, Xu R, Liu JY, Lin C, Yu YY, Xuan DD, Zhu XX, Liu L, Hua YH, Deng CH, Wan WG, Zou HJ, Xue Y. IL-37 blocks gouty inflammation by shaping macrophages into a non-inflammatory phagocytic phenotype. Rheumatology. 2022;61(9):3841–53.
41. He X, Liu J, Zang WJ. Mitochondrial homeostasis and redox status in cardiovascular diseases: protective role of the vagal system. Free Radic Biol Med. 2022;178:369–79.
42. Yu T, Robotham JL, Yoon Y. Increased production of reactiveoxygen species in hyperglycemic conditions requires dynamic changeofmitochondrial morphology.Proceedings of the National Academy ofSciences of the United States of America2006;103(8):2653-8.
43. Tilokani L, Nagashima S, Paupe V, Prudent J. Mitochondrial dynamics: overview of molecular mechanisms. Essays Biochem. 2018;62(3):341–60.
44. Hall AR, Burke N, Dongworth RK, Hausenloy DJ. Mitochondrial fusion and fission proteins: novel therapeutic targets for combating cardiovascular disease. Brit J Pharmacol. 2014;171(8):1890–906.
45. Hu C, Huang Y, Li L. Drp1-Dependent mitochondrial fission plays critical roles in physiological and pathological progresses in mammals. Int J Mol Sci. 2017;18(1).
46. Gandre-Babbe S, van der Bliek AM. The novel tail-anchored membrane protein Mff controls mitochondrial and peroxisomal fission in mammalian cells. Mol Biol Cell. 2008;19(6):2402–12.
47. Kraus F, Roy K, Pucadyil TJ, Ryan MT. Function and regulation of the divisome for mitochondrial fission. Nature. 2021;590(7844):57–66.
48. Yonashiro R, Ishido S, Kyo S, Fukuda T, Goto E, Matsuki Y, Ohmura-Hoshino M, Sada K, Hotta H, Yamamura H, Inatome R, Yanagi S. A novel mitochondrial ubiquitin ligase plays a critical role in mitochondrial dynamics. EMBO J. 2006;25(15):3618–26.
49. Karbowski M, Neutzner A, Youle RJ. The mitochondrial E3 ubiquitin ligase MARCH5 is required for Drp1 dependent mitochondrial division. J Cell Biol. 2007;178(1):71–84.
50. Xu S, Cherok E, Das S, Li SA, Roelofs BA, Ge SX, Polster BM, Boyman L, Lederer WJ, Wang CX, Karbowski M. Mitochondrial E3 ubiquitin ligase MARCH5 controls mitochondrial fission and cell sensitivity to stress-induced apoptosis through regulation of MiD49 protein. Mol Biol Cell. 2016;27(2):349–59.
51. Park YY, Cho H. Mitofusin 1 is degraded at G2/M phase through ubiquitylation by MARCH5. Mol Biol Cell. 2012;23.
52. Kim HJ, Nagano Y, Choi SJ, Park SY, Kim H, Yao TP, Lee JY. HDAC6 maintains mitochondrial connectivity under hypoxic stress by suppressing MARCH5/MITOL dependent MFN2 degradation. Biochem Biophys Res Commun. 2015;464(4):1235–40.
53. Wang R, Xu H, Tan B, Yi Q, Sun Y, Xiang H, Chen T, Liu H, Xie Q, Wang L, Tian J, Zhu J. SIRT3 promotes metabolic maturation of human iPSC-derived cardiomyocytes via OPA1-controlled mitochondrial dynamics. Free Radic Biol Med. 2023;195:270–82.
54. Yi XL, Guo WA, Shi Q, Yang YQ, Zhang WG, Chen XG, Kang P, Chen JX, Cui TT, Ma JY, Wang HN, Guo S, Chang YQ, Liu L, Jian Z, Wang L, Xiao Q, Li SL, Gao TW, Li CY. SIRT3-Dependent mitochondrial dynamics Remodeling contributes to oxidative stress-Induced Melanocyte Degeneration in Vitiligo. Theranostics. 2019;9(6):1614–33.
55. Su ZDZ, Li CQ, Wang HW, Zheng MM, Chen QW. Inhibition of DRP1-dependent mitochondrial fission by Mdivi-1 alleviates atherosclerosis through the modulation of M1 polarization. J Transl Med. 2023;21(1).
56. Rong R, Yang R, Li H, You M, Liang Z, Zeng Z, Zhou R, Xia X, Ji D. The roles of mitochondrial dynamics and NLRP3 inflammasomes in the pathogenesis of retinal light damage. Ann N Y Acad Sci. 2022;1508(1):78–91.
57. Zhou W, Hu GL, He JL, Wang TS, Zuo Y, Cao Y, Zheng Q, Tu J, Ma J, Cai R, Chen YL, Fan QJ, Dong BJ, Tan HS, Wang Q, Xue W, Cheng JK. SENP1-Sirt3 signaling promotes alpha-ketoglutarate production during M2 macrophage polarization. Cell Rep. 2022;39(2).
58. Wang M, Li R, Qi H, Pang L, Cui L, Liu Z, Lu J, Wang R, Hu S, Liang N, Tao Y, Dalbeth N, Merriman TR, Terkeltaub R, Yin H, Li C. Metabolomics and Machine Learning Identify Metabolic Differences and Potential Biomarkers for Frequent versus Infrequent Gout Flares. Arthritis Rheumatol. 2023.

Publisher's Note